PERGAMON

International Journal of Solids and Structures 40 (2003) 2267–2300

INTERNATIONAL JOURNAL OF SOLIDS and STRUCTURES

www.elsevier.com/locate/ijsolstr

A physically based continuum damage mechanics model for thin laminated composite structures

Kevin V. Williams [a], Reza Vaziri [b,*], Anoush Poursartip [b]

[a] *Structural Dynamics and Simulation Group, Weapons Effects Section, Defence R&D Canada—Valcartier, 2459 Pie-XI Blvd., North, Val-Bélair, QC, Canada G3J 1X5*

[b] *Composites Group, Departments of Civil Engineering and Metals and Materials Engineering, The University of British Columbia, Vancouver, BC, Canada V6T 1Z4*

Received 4 December 2001; received in revised form 11 December 2002

Abstract

The present work focuses on the development, implementation, and verification of a plane-stress continuum damage mechanics (CDM) based model for composite materials. A physical treatment of damage growth based on the extensive body of experimental literature on the subject is combined with the mathematical rigour of a CDM description to form the foundation of the model. The model has been implemented in the commercial finite element code, LS-DYNA and the results of the application of the model to the prediction of impact damage growth and its effects on the impact force histories in carbon fibre reinforced plastic laminates are shown to be physically meaningful and accurate. Furthermore, it is demonstrated that the material characterization parameters can be extracted from the results of standard test methodologies for which a large body of published data already exists for many composite materials.

Keywords: Continuum damage mechanics; Constitutive model; Composites; Damage growth; Energy absorption; Impact

1. Introduction

1.1. Background

Attempt to address the issue of damage growth in laminated fibre-reinforced plastic (FRP) composites have been made by an ever-increasing number of researchers through the use of continuum damage mechanics (CDM). Simply stated, CDM attempts to predict the effect of microscale defects and damage at a macroscale by making assumptions about the nature of the damage and its effect on the macroscale properties (e.g. modulus) of the material (Kachanov, 1958, 1986; Krajcinovic, 1984, 1996; and Ortiz, 1985, among others). The basis for the stress–strain relationship in many CDM approaches is the concept of strain, stress, or energy equivalence (Simo and Ju, 1987; Chaboche, 1988a,b; Chow and Wang, 1987; Kennedy and Nahan,

* Corresponding author. Tel.: +1-604-822-2800; fax: +1-604-822-6901.
E-mail addresses: kevin.williams@drdc-rddc.gc.ca (K.V. Williams), reza.vaziri@ubc.ca (R. Vaziri).

0020-7683/02/$ - see front matter © 2002 Elsevier Science Ltd. All rights reserved.
doi:10.1016/S0020-7683(03)00016-7

1997; Krajcinovic, 1984, 1996; Lemaître and Chaboche, 1978; Yazdchi et al., 1996). In the commonly used strain equivalence approach, a material containing damage, subjected to a strain, ε, and under a state of stress, σ, can be represented as an equivalent undamaged material subject to the same strain, ε, but under an effective stress state, $\hat{\sigma}$. This can be expressed mathematically by the relation:

$$\{\hat{\sigma}\} = [M(\omega)]\{\sigma\} \tag{1}$$

where $[M(\omega)]$ is a transformation tensor which is a function of the damage state, ω, and $\{\sigma\}$, $\{\hat{\sigma}\}$ are the actual stress and equivalent stress tensors. Note that here and throughout the paper the symmetric second-order and fourth-order tensors are written in Voigt matrix notation.

Introducing the effective stress–strain relationship, $\{\hat{\sigma}\} = [C^0]\{\varepsilon\}$, into Eq. (1), we obtain:

$$\{\sigma\} = [M]^{-1}[C^0]\{\varepsilon\} = [C(\omega)]\{\varepsilon\} \tag{2}$$

where $[C^0]$ is the constitutive or stiffness tensor of the undamaged material and $[C(\omega)]$ is the damaged or effective stiffness tensor. The entries of $[C(\omega)]$ are the elastic coefficients, which are functions of the undamaged (or initial) elastic material constants and the damage state ω.

The role of a CDM model is to provide a mathematical description of the dependence of these elastic coefficients (i.e. the residual stiffness functions) on the damage state and of the change in the damage state, ω, with load state. The damage variable ω is typically expressed as a function of the strain and/or the strain rate through a scalar-valued history parameter r; i.e. $\omega = \omega(r)$. The parameter r assumes a role similar to the flow stress in incremental plasticity theory and obeys a loading function f in the strain space, $f = F(\varepsilon) - r$, where F is a scalar potential function of the strain components (i.e. an effective strain). The damage threshold, r, which in multiaxial loading case determines the size of the damage surface can be a function of both strain and strain-rate to account for potential rate dependency of the damage. The key to the success of all CDM models is to maintain a coherent link with the physical observations of damage growth and material response.

1.2. Motivation for model development

As a preliminary step in the development of a new CDM model, an existing composite damage model due to Matzenmiller et al. (1995) was implemented in the explicit finite element code, LS-DYNA (Williams and Vaziri, 1995, 2001). The purpose here was not to judge this model against other CDM theories but rather to compare the predictions made by a CDM approach with a more traditional composite failure model.

Williams and Vaziri (1995, 2001) evaluated the Matzenmiller et al. (MLT) model based on a series of numerical analyses performed to predict the response of T800H/3900-2 carbon FRP (CFRP) composite plates subject to non-penetrating normal impacts of various incident energy levels. The implementation of the CDM-based composite damage model demonstrated significant improvements in the prediction of damage growth and force and energy-time histories when compared to an existing composite failure model in LS-DYNA. While results of the application of this model demonstrate that CDM provides a useful framework for further development of damage models for laminated structures, a number of issues were raised during the investigation, which should be addressed by a new damage model. These include:

- the physical significance of the choice of damage parameter,
- ease of material characterization,
- stacking sequence or lay-up dependence of the damage growth in laminated structures,
- rate dependence, and
- mesh size dependence of the predicted damage growth.

The first three items are all related and are dealt with in some detail in this paper. The latter two items were deemed to be beyond the scope of the present work. This is not to say, however, that their importance is being downplayed. Rather, a reasonable structure for the model must first be developed before they can be adequately addressed.

2. Model formulation

Our approach in the development of a new 3D CDM model for composites (Williams, 1998) has been to divide the problem into two components; one concentrating on the in-plane response (the subject of this paper) and the other on the out-of-plane or through-thickness response (see Floyd et al., 1999). Not only does this simplify the formulation but also the model development is significantly quicker as one does not have the computational overhead of running full 3D models during the iterative model development phase. This work represents the first stage in the ongoing development of a family of CDM-based models, under the general title CODAM (composite damage model). The remainder of this section is devoted to the formulation of the plane-stress CODAM3D**s** (i.e. shell element based) model.

2.1. Sub-structuring

The first feature of our approach is to treat the material as an orthotropic medium made up of a series of repeating units through the thickness. Typically, constitutive models applicable to composite materials have treated the composite as a stack of perfectly bonded unidirectional laminae (Chang and Chang, 1987; Matzenmiller et al., 1995; Pickett et al., 1990). These models are based on the lamina behaviour and the response of the bulk material is assumed to follow the first order shear deformable laminated plate theory (constant shear through the thickness resulting in limited interaction between layers). Experimental observations, supported by analytical and numerical modelling, have clearly shown that the failure mode, and hence the response of laminated composite materials is closely linked to the stacking sequence and lamina interactions (see for example Dost et al., 1991; Lagace, 1984; Pagano and Pipes (1971)). The orientation of the neighbouring plies play a major role in the response of a lamina particularly in the inelastic regime where damage initiation and evolution in the lamina strongly depend on the level of confinement provided by the adjacent plies in the laminate. In other words, the response of a single lamina in a stack is governed by its in-situ characteristics. Generally, a laminate is made up of a number of repeating units (sub-laminates) through the thickness. These sub-laminates largely control the lamina interactions caused by the stacking sequence. As a result, a model constructed at this scale has the potential to incorporate these interactions.

From an implementation point of view, the differences between the lamina and sub-laminate approaches are relatively minor. Plane stress shell elements use through-thickness integration points to evaluate bending stresses (shown schematically in Fig. 1). These integration points are used in lamina models by associating the appropriate local material angle with each integration point. The resulting laminate response prediction is analogous to that obtained from a laminated plate theory type analysis. The sub-laminate approach uses the same technique although in most cases a material angle is not required. Typically a minimum of one integration point would be used for each sub-laminate. The exception is a thin laminate where the minimum number of integration points required to accurately capture the bending response may determine the number of points used. Overall, fewer integration points are required, hence increasing the efficiency of the model, and the interactions of the laminae are incorporated in the sub-laminate constitutive behaviour, thus improving the accuracy of the prediction.

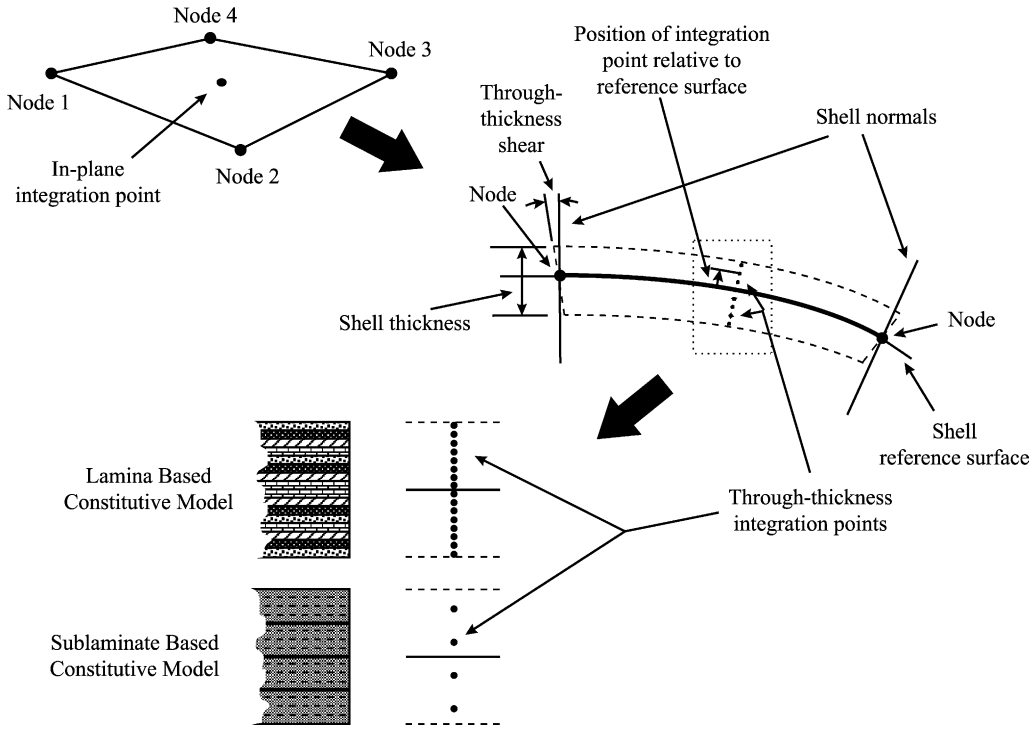

Fig. 1. Shell representation of a laminated composite using a lamina and sub-laminate based constitutive model.

2.2. Selection of damage parameters

Traditionally damage parameters are associated with cracking (e.g. reduction in the cross sectional area of the load bearing material) in the principal lamina directions, parallel and perpendicular to the fibre direction, corresponding to matrix and fibre dominated damage modes. At the sub-laminate scale there is no clearly defined directionality of the damage modes in arbitrary lay-ups. The problem is simplified if we consider only symmetric laminates ($[0/\pm45/90]_{nS}$, $[\pm60]_{nS}$ and $[0/90_n]_S$ for example), where there exists at least a material symmetry at the sub-laminate level. By defining two damage parameters, ω_x and ω_y, aligned with the sub-laminate co-ordinate system it is possible to characterize the damage state as projections of the crack densities normalized to the saturation crack density in the principal material directions.

While adequately describing the effect of matrix cracking and fibre failure on E_x and E_y in simple cross-ply laminates (i.e. $[0_n/90_m]_{nS}$), there is a need to define an additional damage term to model the interactive effect of the two damage parameters on shear modulus in more general symmetric lay-ups (e.g. $[0/\pm45/90]_{nS}$). A survey of approaches taken to this problem in other CDM models shows a somewhat varied treatment, e.g. the following two distinct formulations have been used for shear modulus of a damaged composite within the common framework of energy equivalent CDM:

$$G_{12} = (1-\omega_1)(1-\omega_2)G_{12}^0 \quad \text{Chow and Wang (1987)} \tag{3}$$

$$G_{12} = \frac{2(1-\omega_1)^2(1-\omega_2)^2}{(1-\omega_1)^2+(1-\omega_2)^2}G_{12}^0 \quad \text{Yazdchi et al. (1996)} \tag{4}$$

Note that both of these are lamina based with indices 1 and 2 referring to the principal material directions in the lamina. Matzenmiller et al. (1995) take a somewhat unconventional approach of introducing a completely independent 'shear damage parameter', ω_s, with an associated damage threshold and growth law. Although less physical, this approach avoids the difficulty associated with defining an interactive term.

If Eq. (3) were to be used as a basis for shear modulus reduction due to damage, then ω_s would take the following form:

$$\omega_s = \omega_x + \omega_y - \omega_x\omega_y \tag{5}$$

However, at intermediate levels of damage, this function predicts a more significant effect of the damage state on shear than on either of the principal directions. For example, with $\omega_x = 0.5$ and $\omega_y = 0.5$ one might expect ω_s to be on the order of 0.5 but Eq. (5) results in $\omega_s = 0.75$, a significantly higher value. By modifying Eq. (5) slightly such that:

$$\omega_s = \sqrt{\omega_x^2 + \omega_y^2 - \omega_x\omega_y} \tag{6}$$

then one obtains the more reasonable result of $\omega_s = 0.50$. The latter is the formulation adopted here for the damage parameter associated with shear modulus reduction.

2.3. Damage growth law

One of our main concerns with the MLT approach is the use of a single mathematical expression to describe the damage evolution as a function of strain over the entire load range, an approach which is characteristic of many CDM models. Combining this with a linearly varying modulus reduction as a function of damage results in a strain-softening type stress–strain curve that is non-linear (corresponding to a damaging material) over the entire range of strains. In other words, the ascending and descending branches of the stress–strain curve are coupled (i.e. the Weibull parameter m controls the entire shape of the curve) thus restricting the versatility of the model to represent different amounts of softening without affecting the elastic response and peak stress value.

We adopt a more versatile and physically meaningful approach where we consider three behaviour regimes or zones in the material response: (i) undamaged elastic, (ii) damage phase 1 (matrix/delamination dominated), and (iii) damage phase 2 (fibre and matrix/delamination dominated). Each is characterized by a different relationship between the damage variables ω_i $(i = x, y)$ and the corresponding load state defined by scalar potential functions F_i. In keeping with experimental observations (e.g. Delfosse and Poursartip, 1997), the present model assumes that matrix damage is closely associated with delamination so that quantification of matrix damage leads to a good estimate of the delamination area.

The simplest and most flexible approach to capture the changes in damage growth is to assume a linear relationship within each of these regions (e.g. Pickett et al., 1990). First consider the matrix damage. We define a threshold value for damage initiation $r_0 = F^{\mathrm{I}}$ marking the end of the elastic response and the onset of matrix damage ($\omega^{\mathrm{I}} = 0$ at F^{I}).

The assumption of decoupled fibre and matrix damage growth means that, regardless of any fibre damage which may develop, the matrix damage will continue to grow linearly with damage up to rupture defined by the ultimate damage threshold $r_f = F^{\mathrm{III}}$ where $\omega^{\mathrm{III}} = 1$ (see Fig. 2). The total amount of damage attributed to matrix cracking and delamination, ω'_m, will be some value less than 1.0, determined by the lay-up of the sub-laminate.

Following the same argument for fibre breakage, we define F^{II} as the threshold for onset of fibre damage and $\omega'_f = 1 - \omega'_m$ as the proportion of the total damage attributed to fibre failure. The net damage

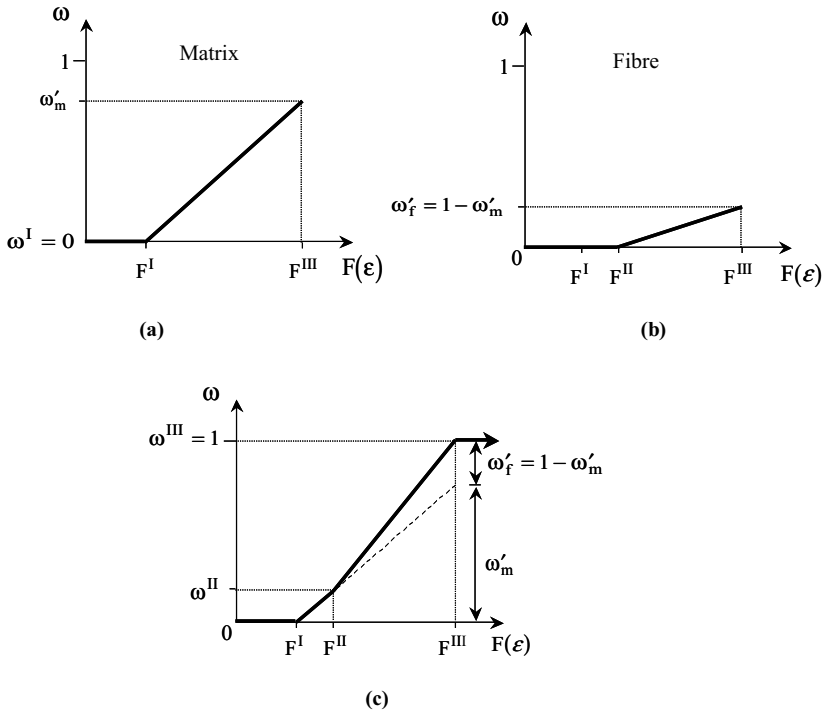

Fig. 2. Construction of the bilinear damage growth law (c) based on the combined contributions of (a) matrix and delamination damage and (b) fibre breakage.

growth function results from the superposition of these two functions as shown in Fig. 2. Note that the damage state ω^{II} at the transition between the two phases of damage growth is not an independent parameter. Rather, it is dependent on the values of F^{I}, F^{II}, F^{III}, and ω'_m (ω'_f being a function of ω'_m) such that:

$$\omega^{\mathrm{II}} = \omega'_m\left(\frac{F^{\mathrm{II}} - F^{\mathrm{I}}}{F^{\mathrm{III}} - F^{\mathrm{I}}}\right) \tag{7}$$

The resulting piece-wise linear relation between ω and F is shown in Fig. 2. ω, as a function of the load state is:

$$\omega = \begin{cases} 0 & 0 < F \leqslant F^{\mathrm{I}} \\ \omega^{\mathrm{II}}\left(\dfrac{F - F^{\mathrm{I}}}{F^{\mathrm{II}} - F^{\mathrm{I}}}\right) & F^{\mathrm{I}} < F \leqslant F^{\mathrm{II}} \\ \omega^{\mathrm{II}} + (1 - \omega^{\mathrm{II}})\left(\dfrac{F - F^{\mathrm{II}}}{F^{\mathrm{III}} - F^{\mathrm{II}}}\right) & F^{\mathrm{II}} < F \leqslant F^{\mathrm{III}} \\ 1 & F > F^{\mathrm{III}} \end{cases} \tag{8}$$

It is important to note that in keeping with the thermodynamic constraints in damage mechanics, damage is considered to be an irreversible process and therefore ω is a monotonically increasing function of time t such that:

$$\omega = \max[\omega^{\tau} | \tau \leqslant t,\ \omega^{t}] \tag{9}$$

where ω^t is the damage calculated from Eq. (8) for the current load state, and ω^τ represents the state of damage at previous times $\tau \leqslant t$. Clearly, the evolution of the damage threshold can be mathematically expressed as

$$r = \max[F^\tau | \tau \leqslant t,\ r_0] \tag{10}$$

and the loading–unloading conditions follow the Kuhn–Tucker conditions:

$$\dot{r} \geqslant 0, \quad f \leqslant 0, \quad \dot{r}f = 0 \tag{11}$$

where $f = F - r$ and overdot denotes differentiation with respect to time.

In the above discussion, the second phase of damage is assumed to incorporate both matrix damage and fibre damage. There are three other possibilities that should be identified: (1) the first mode of damage saturates at or before the onset of the second, (2) the first mode saturates after the onset of the second but before rupture, and (3) the second mode of damage saturates before rupture. The first two cases can be used to describe the response of a $[0_n/90_m]_S$ laminate, for example. Matrix/delamination damage in brittle matrix cross-ply laminates can saturate before the onset of fibre failure while fibre breakage will typically initiate before matrix cracking saturation in a tough matrix FRP system. The limit is the case considered in this paper where matrix/delamination damage continues to grow until rupture.

The behaviour described by the third case represents a material where fibre damage is arrested, either by a physical mechanism (a toughening of the response) or by a change in the load state resulting from the softening of the sub-laminate and/or the decoupling of the plies. For example, it is conceivable that growth of a significant amount of delamination damage can allow individual plies to decouple and rotate, aligning the fibre directions with the principal loading direction without driving more fibre damage.

These three additional damage growth behaviours are characterized by a three-phase (i.e. trilinear) response. For the purposes of this paper we are assuming that the two-phase damage growth model applies. The extension of the model to cover these more mathematically (not physically) complex material responses is being actively pursued (e.g., Floyd et al., 2001) as it is largely a coding issue and the theoretical foundation of the model remains the same.

2.4. Damage potential function

In general, the damage potential function, F, which is the driving force for damage growth, can be a function of the strains (or stresses). The selection of the damage potential function is the least physical component of the present model. A number of approaches can be taken including the use of strength-based failure criteria such as those presented by Tsai and Wu (1971) or Hashin (1980). The appropriate choice of a mathematical function for predicting failure (initial and final) of FRP laminates is still a subject of much debate among the leading researchers in the composites community. A recent "world wide failure exercise" organized by Hinton et al. (Hinton and Soden, 1998; Soden et al., 1998; Hinton et al., 2001) was launched to assess the predictive capability of some of the most established failure theories available in the literature. The outcome of this study was that even for seemingly simple test cases there was a fairly wide discrepancy between the various predictions and test results suggesting that the subject of failure theories is still far from being mature.

Among the many possibilities available, the potential function in our model is assumed to be an equivalent strain given by a function of local strain components that has the following general form:

$$F = \sqrt{\left(\frac{\varepsilon_x}{K}\right)^2 - \left(\frac{\varepsilon_x}{K}\right)\left(\frac{\varepsilon_y}{L}\right) + \left(\frac{\varepsilon_y}{L}\right)^2 + \left(\frac{\gamma_{xy}}{S}\right)^2 + \left(\frac{\gamma_{yz}}{T}\right)^2 + \left(\frac{\gamma_{zx}}{U}\right)^2} \tag{12}$$

For simplicity, rate effects on the values of the threshold parameter r in the loading function $f = F - r$ are ignored. This limits the initial application of the model to rate insensitive materials such as CFRP and, to a lesser degree, glass fibre-reinforced plastic (GFRP) composites.

Eq. (12) describes an ellipsoidal surface in the strain space (similar to distortional energy-based failure criteria). The two out-of-plane shear strain terms have been added so as to account for all the strains that can contribute to damage growth in a shear deformable shell element formulation used in this study (see Section 5.4). Here the constants K, L, S, T, and U are not used as measures of strength but rather as scalars to provide a measure of the relative contribution of each strain component to the driving force for damage growth. The relative effect of tensile and compressive loading on the damage growth is also introduced through the damage potential functions by introducing a separate set of constants for tension and compression (e.g. K_t if $\varepsilon_x \geqslant 0$ and K_c if $\varepsilon_x < 0$).

The incorporation of through-thickness shear terms accounts for the effects of the γ_{yz} and γ_{zx} strains on the initiation of delamination damage in a plate subject to bending loads. These strains, along with the through-thickness strain, ε_z, are also responsible for edge effects in laminated composites. Delamination growth can be initiated by an incompatibility of the through-thickness strain (stress) field between neighbouring plies of mismatched angle at a discontinuity such as the edge of a laminated plate subjected to bending and/or in-plane loading. However, by smearing the through-thickness anisotropy of the sub-laminates, the model becomes insensitive to these effects under purely in-plane loading. The through-thickness strain has not been included in the potential function because in a plane stress shell formulation ε_z is merely a weighted sum of the in-plane strains, which have already been accounted for in Eq. (12), i.e.

$$\varepsilon_z = -(\nu_{xz}\varepsilon_x + \nu_{yz}\varepsilon_y) \tag{13}$$

However, the ε_z term becomes very important in 3D formulations where it is no longer a simple function of the in-plane strains. Local tensile and compressive through-thickness strains serve to promote and inhibit delamination growth, respectively. These strains can result from contact forces for example.

2.5. Effect of damage on elastic constants

The amount of damage sustained by the sub-laminate will affect each of the material moduli to varying degrees. Many lamina based CDM models developed for composites assume that the loss of modulus is linear with damage (refer to Fig. 3a):

$$R_{E_i} = \frac{E_i}{E_i^0} = (1 - k_i\omega_i) \tag{14}$$

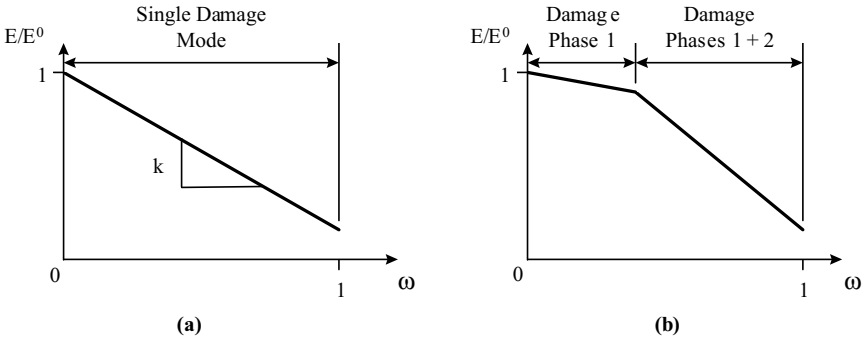

Fig. 3. Modulus variation according to (a) linear and (b) bilinear normalized residual stiffness functions.

where R_{E_i} is the normalized residual modulus (modulus of the damaged material) in the ith direction, E_i is the residual modulus, E_i^0 is the undamaged modulus, and k_i ($k_i \leqslant 1$) are constants that define the rate of modulus loss with the damage, ω_i. This simple relationship is possible because the lamina moduli are only dependent on the damage parameter associated with the appropriate principal material direction. That is, the longitudinal stiffness (E_1) is dominated by fibre breakage (defined by ω_1) and the transverse stiffness (E_2) by matrix damage (ω_2). However, in a sub-laminate, the modulus reduction is a function of both matrix and fibre damage (refer to the discussion above in Section 2.3). One would expect the rate of stiffness loss associated with matrix/delamination damage and fibre breakage to be different. Therefore, the modulus loss is assumed to be a bilinear function of the damage parameter (Fig. 3b). A bilinear representation of the residual modulus function was also used by Pickett et al. (1990) although it was not applied at this scale nor did the damage parameters have the same meaning.

This approach is supported by the work of Poursartip et al. (1986), for example, who showed that the stiffness loss due to matrix damage and delamination was linear with damage density in a $[45/90/-45/0]_S$ laminate subjected to fatigue loading (i.e. stable crack growth). After a certain level of damage was reached, corresponding to a 35% stiffness loss in the particular CFRP system investigated, a change in mechanism was observed. Poursartip et al. attributed this to the initiation of fibre dominated failure and, based on the work by Steif (1984) on stiffness reduction due to fibre breakage, proposed that a second 'leg' could be added to the overall stiffness reduction function to reflect the additional effect of fibre failure. Steif (1984) has shown further that the relationship between stiffness loss and fibre breakage density is a linear function.

Following this approach we define a general bilinear curve to describe the modulus loss with damage as shown in Fig. 4. The normalized reduced stiffness at saturation of matrix/delamination damage, R'_E, is associated with the corresponding level of damage ω'_m (defined in Section 2.3). Plotting this point on Fig. 4 establishes the slope of the residual stiffness curve associated with matrix/delamination damage. Identifying the onset of fibre damage (defined by ω^{II}) on Fig. 4, the corresponding normalized residual stiffness can be evaluated as:

$$E^{II} = 1 - (1 - R'_E)\frac{\omega^{II}}{\omega'_m} \tag{15}$$

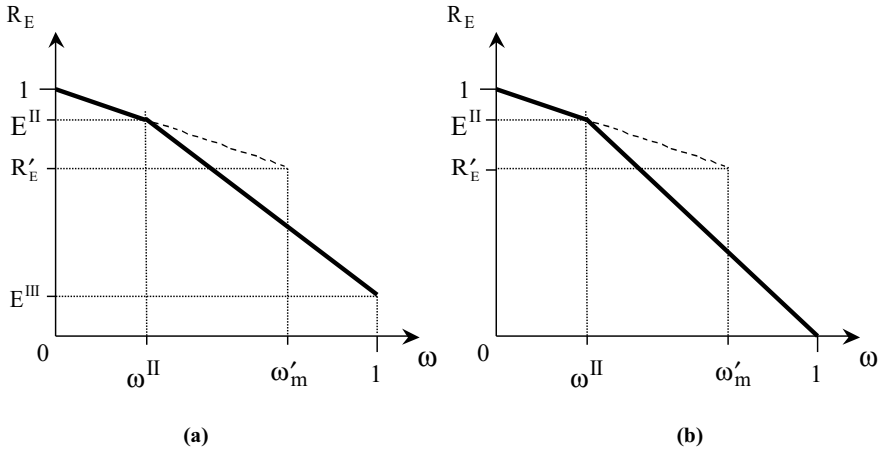

Fig. 4. Bilinear residual stiffness curve showing modulus loss (E/E^0) versus damage (ω) relationship: (a) generalized function with a residual modulus and (b) special case with saturation of damage at rupture ($\omega^{III} = 0$ and $E^{III} = 0$).

Given the orthotropic nature of the material, independent functions need to be defined for reduction of elastic constants:

$$E_x = R_{E_x}(\omega_x)E_x^0; \quad E_y = R_{E_y}(\omega_y)E_y^0; \quad G_{xy} = R_{G_{xy}}(\omega_x,\omega_y)G_{xy}^0; \quad \text{and} \quad v_{xy} = R_{v_{xy}}(\omega_x,\omega_y)v_{xy}^0 \tag{16}$$

where the normalized reduction function, $R_X(\omega)$, with X denoting any one of the orthotropic elastic constants, takes the following generalized form (see Fig. 4):

$$R_X = \begin{cases} 1 + (X^{\mathrm{II}} - 1)\dfrac{\omega}{\omega^{\mathrm{II}}} & 0 < \omega \leqslant \omega^{\mathrm{II}} \\ X^{\mathrm{II}}\left(\dfrac{1-\omega}{1-\omega^{\mathrm{II}}}\right) & \omega^{\mathrm{II}} < \omega \leqslant 1 \end{cases} \tag{17}$$

Here the assumption is made that complete damage will result in total stiffness loss (i.e. $E = 0$ when $\omega = 1$). Potential differences in stiffness loss under tensile and compressive loading are incorporated by allowing independent definitions of the normalized residual modulus functions for the Young's moduli for each loading condition.

Poisson's ratio v has not been included in the discussions leading to Eq. (17) because the degradation of this interaction term is not independent of the functions chosen for the moduli E_x and E_y. The major symmetry of the constitutive stiffness and compliance tensors must be retained both for an undamaged and damaged material, and as a result the following reciprocity relationship must hold:

$$\frac{v_{xy}^0}{E_x^0} = \frac{v_{yx}^0}{E_y^0} \quad \text{and} \quad \frac{v_{xy}}{E_x} = \frac{v_{yx}}{E_y} \tag{18}$$

Therefore:

$$\frac{R_{v_{xy}}(\omega_x,\omega_y)v_{xy}^0}{R_{E_x}(\omega_x)E_x^0} = \frac{R_{v_{yx}}(\omega_x,\omega_y)v_{yx}^0}{R_{E_y}(\omega_y)E_y^0} \quad \text{and} \quad \frac{R_{v_{xy}}(\omega_x,\omega_y)}{R_{E_x}(\omega_x)} = \frac{R_{v_{yx}}(\omega_x,\omega_y)}{R_{E_y}(\omega_y)} \tag{19}$$

One possible solution, albeit not unique, would be to have:

$$R_{v_{xy}}(\omega_x,\omega_y) = R_{E_x}(\omega_x) \quad \text{and} \quad R_{v_{yx}}(\omega_x,\omega_y) = R_{E_y}(\omega_y) \tag{20}$$

The modulus degradation functions applied to v_{xy} and v_{yx} must be the same functions of ω_x and ω_y that are applied to E_x and E_y, respectively. Experimental evidence for the effects of damage on Poisson's ratio is rare, possibly because of the difficulties associated with measuring v_{xy} in specimens with progressive damage development. However, Camponeschi and Stinchcomb (1982) provide some evidence that the reduction in v_{xy} measured during fatigue loading of quasi-isotropic CFRP laminates is of the same order and follows the same trends as the reduction in E_x.

In the present approach the effect of delamination is included in the overall effect of matrix damage on the in-plane elastic constants (e.g. a reduction of E corresponding to a reduction in bending stiffness and the reduction of G and v corresponding to decoupling or a release of the constraint between neighbouring laminae within the sub-laminate).

2.6. Constitutive relationship

Having defined the normalized residual stiffness functions, we can now return to the constitutive equation and derive the final form of the plane stress constitutive equation:

$$\{\sigma\} = [C]\{\varepsilon\} = \begin{bmatrix} C_{11} & C_{12} & 0 \\ C_{21} & C_{22} & 0 \\ 0 & 0 & C_{66} \end{bmatrix} \begin{Bmatrix} \varepsilon_x \\ \varepsilon_y \\ \gamma_{xy} \end{Bmatrix} \tag{21}$$

where the coefficients of the constitutive secant stiffness tensor, C_{ij}, are functions of the damage state, $R_E(\omega_x, \omega_y)$, and the undamaged elastic constants, E^0, G^0, and v^0.

It is convenient to approach the problem of deriving these coefficients using the compliance tensor, $[H] = [C]^{-1}$ given by:

$$[H] = \begin{bmatrix} \dfrac{1}{E_x} & -\dfrac{v_{xy}}{E_x} & 0 \\ -\dfrac{v_{yx}}{E_y} & -\dfrac{1}{E_y} & 0 \\ 0 & 0 & \dfrac{1}{G_{xy}} \end{bmatrix} \tag{22}$$

Substituting for the damaged elastic constants from Eq. (16), and using the relationships developed for $R_{v_{xy}}$ and $R_{v_{yx}}$ in Eq. (20) we obtain the final form of the constitutive stiffness tensor:

$$[C] = \begin{bmatrix} \dfrac{R_{E_x}E_x^0}{(1 - R_{E_x}R_{E_y}v_{xy}^0 v_{yx}^0)} & \dfrac{R_{E_x}R_{E_y}E_y^0 v_{xy}^0}{(1 - R_{E_x}R_{E_y}v_{xy}^0 v_{xy}^0)} & 0 \\ & \dfrac{R_{E_y}E_y^0}{(1 - R_{E_x}R_{E_y}v_{xy}^0 v_{yx}^0)} & 0 \\ \text{SYM} & & R_{G_{xy}}G_{xy}^0 \end{bmatrix} \tag{23}$$

Note that the functions R_X vary between 1 and 0. As a result, the constitutive tensor is positive definite over the entire range of damage.

2.7. 1D Stress–strain relationship

To better illustrate the features of the model let us consider the resulting stress–strain response for a one-dimensional case. First, we will construct the stress–strain relationships for each of the three zones: undamaged elastic (stage 1), onset of the first damage phase (stage 2), and onset of the second damage phase (stage 3).

In the one-dimensional case, the damage potential function becomes:

$$F(\varepsilon) = \sqrt{\left(\frac{\varepsilon}{1}\right)^2} = \varepsilon \tag{24}$$

Substituting into Eq. (8) one obtains:

$$\omega = \begin{cases} 0 & 0 < \varepsilon \leqslant F^{\mathrm{I}} \\ \omega^{\mathrm{II}}\left(\dfrac{\varepsilon - F^{\mathrm{I}}}{F^{\mathrm{II}} - F^{\mathrm{I}}}\right) & F^{\mathrm{I}} < \varepsilon \leqslant F^{\mathrm{II}} \\ \omega^{\mathrm{II}} + (1 - \omega^{\mathrm{II}})\left(\dfrac{\varepsilon - F^{\mathrm{II}}}{F^{\mathrm{III}} - F^{\mathrm{II}}}\right) & F^{\mathrm{II}} < \varepsilon \leqslant F^{\mathrm{III}} \\ 1 & F^{\mathrm{III}} < \varepsilon \end{cases} \tag{25}$$

In stage 1:

$$\sigma = E^0\varepsilon \quad 0 < \varepsilon < F^{\mathrm{I}} \tag{26}$$

For stage 2, from Eq. (17):

$$\sigma = E\varepsilon = [1 + \left(E^{\mathrm{II}} - 1\right)\frac{\omega}{\omega^{\mathrm{II}}}]E^0\varepsilon \tag{27}$$

which after substitution for ω from Eq. (25) in the range $F^{\mathrm{I}} < \varepsilon \leqslant F^{\mathrm{II}}$ yields:

$$\sigma = \left(\frac{F^{\mathrm{II}} - E^{\mathrm{II}}F^{\mathrm{I}}}{F^{\mathrm{II}} - F^{\mathrm{I}}}\right)E^0\varepsilon + \left(\frac{E^{\mathrm{II}} - 1}{F^{\mathrm{II}} - F^{\mathrm{I}}}\right)E^0\varepsilon^2 \quad F^{\mathrm{I}} < \varepsilon < F^{\mathrm{II}} \tag{28}$$

Similarly for stage 3:

$$\sigma = \left(\frac{E^{\mathrm{II}}F^{\mathrm{III}}}{F^{\mathrm{III}} - F^{\mathrm{II}}}\right)E^0\varepsilon - \left(\frac{E^{\mathrm{II}}}{F^{\mathrm{III}} - F^{\mathrm{II}}}\right)E^0\varepsilon^2 \quad F^{\mathrm{II}} < \varepsilon < F^{\mathrm{III}} \tag{29}$$

For $\varepsilon \geqslant F^{\mathrm{III}}$, $\omega = 1.0$ and hence $E = 0$ and $\sigma = 0$.

The predicted stress–strain response is shown in Fig. 5. The flexibility of the bilinear model is demonstrated in Fig. 6. By varying the damage growth and residual stiffness curves it is possible to obtain a material response that mimics the response predicted by the traditional instantaneous failure models (Fig. 6a), a material response that approaches the statistically based CDM models where the stress is a single continuous function of strain (Fig. 6b), or responses in-between. Fig. 6c shows a response with an elastic region followed by the onset of damage leading to catastrophic failure. Fig. 6d shows the complete response (similar to Fig. 5) with a linear-elastic region, the onset of damage, and finally a softening response. It is interesting to note that the resulting constitutive law is independent of ω^{II}.

The role of the model has been to define the stiffness terms as a function of damage, Eq. (17), and in turn the damage as a function of loading, Eq. (8). In fact, what is implied in the model development is the decomposition of the relationship between the stiffness change and the strain state:

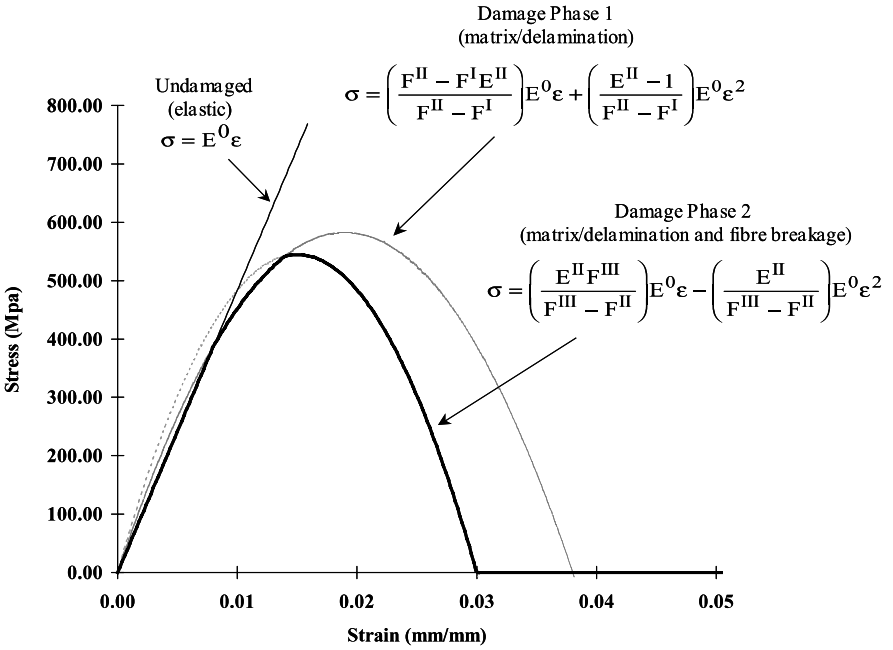

Fig. 5. Predicted one-dimensional stress–strain response based on the combination of bilinear damage growth and bilinear residual stiffness functions.

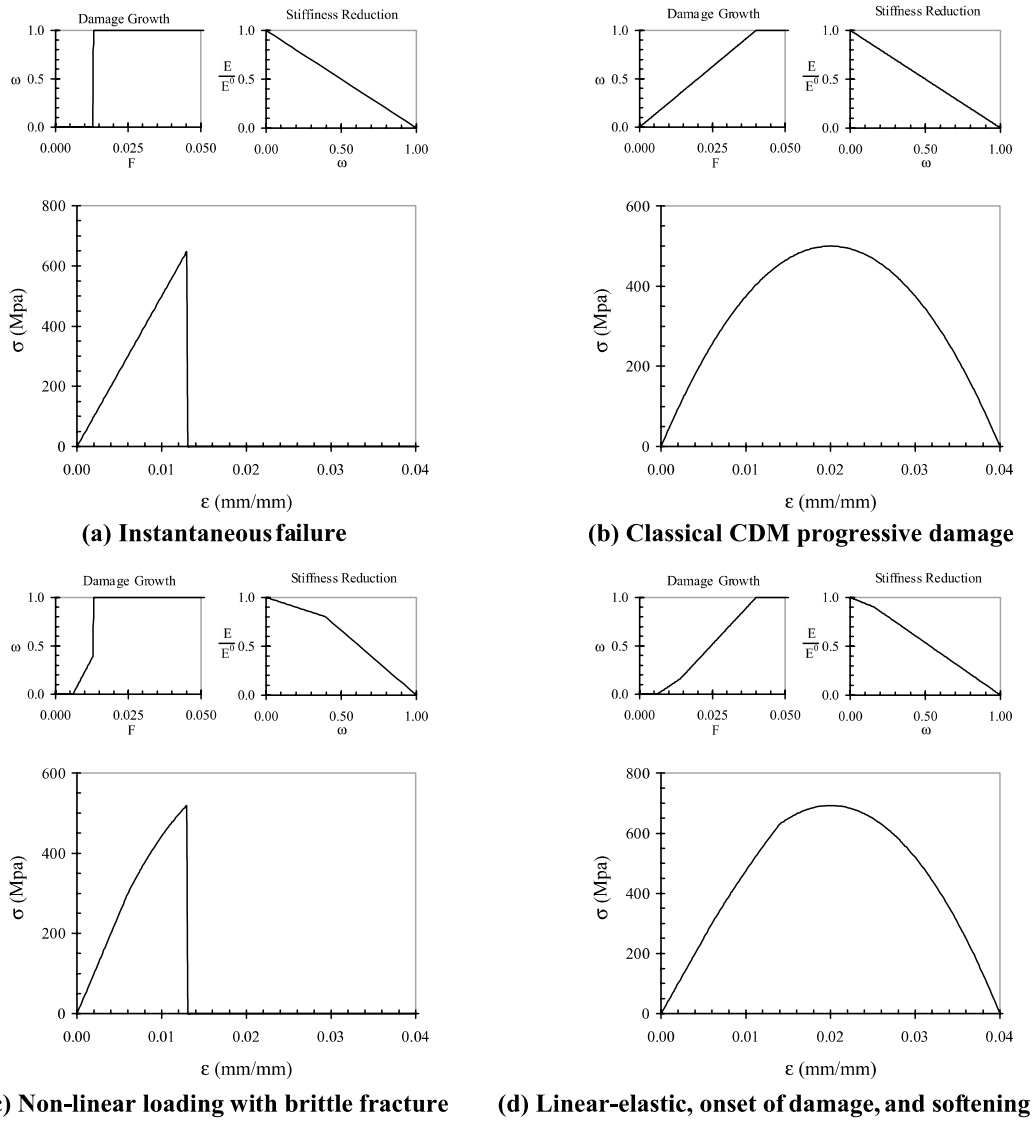

Fig. 6. Examples of predicted one-dimensional stress–strain response for the proposed model CODAM.

$$\frac{\partial E}{\partial \varepsilon} = \frac{\partial E}{\partial \omega} \cdot \frac{\partial \omega}{\partial \varepsilon} \tag{30}$$

where $\partial E/\partial\omega$ and $\partial\omega/\partial\varepsilon$ can be obtained explicitly from Eqs. (17) and (8), respectively. ω is, in fact, an intermediate value which, in itself is convenient as it allows a further interpretation of the resulting degradation of the material properties in terms of a more physical and more easily observed quantity, damage.

The link between the two functions $\partial E/\partial\omega$ and $\partial\omega/\partial\varepsilon$ is ω^{II} or rather ω'_m. The effect of changing ω'_m is shown in Fig. 7. It can be seen that shifting ω'_m while keeping the modulus at saturation of matrix damage, R'_E, constant results in a shift in, ω^{II} defined by the damage growth function. This shift in ω^{II}, when plotted

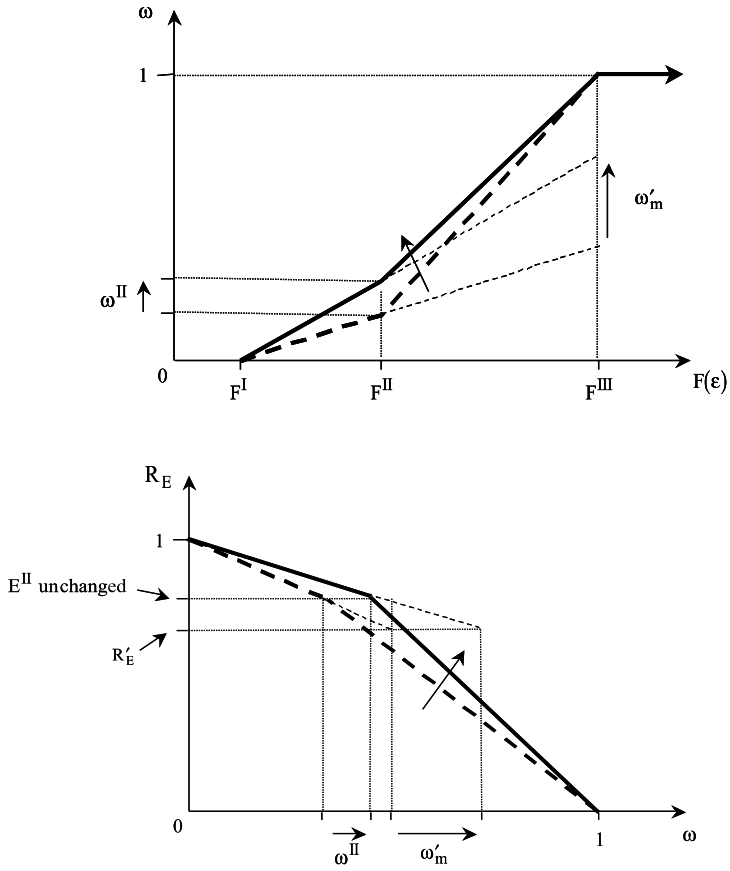

Fig. 7. Effect of changing the damage associated with saturation of matrix cracking on the residual stiffness and damage growth functions.

on the residual stiffness curves results in no change in E^{II}. Note that, although the slopes of both the damage growth and residual stiffness functions change, the value of E^{II} at $F = F^{II}$, and hence the relationship between E and F (or ε), remains the same in both segments of the two functions. The result is that the rate of stiffness loss with strain, $\partial E/\partial\varepsilon$, is independent of ω'_m (or ω^{II}). While its value may not directly influence the predicted response, ω'_m does provide a physical interpretation of the damage growth and stiffness reduction curves in that it allows a more direct characterization of the damage model using the data available in the literature on stiffness reduction.

2.8. Numerical implementation

The CODAM material model described above has been implemented as a user material (UMAT) module for shell elements, in the explicit non-linear finite element code, LS-DYNA (Hallquist et al., 1994). Similar to all other constitutive modules, the CODAM subroutine is strain-driven. Given that the relations between the damage and damage potential in the principal sub-laminate directions $i = x, y$ are defined by the user as input, the algorithmic details at a time station $t_{n+1} = t_n + \Delta t$ and at a given integration point can be summarized as follows:

1. Based on the current strain rates, $\{\dot{\varepsilon}\}_{n+1}$, update the total strains: $\{\varepsilon\}_{n+1} = \{\varepsilon\}_n + \{\dot{\varepsilon}\}_{n+1}\Delta t$.
2. Compute the effective strain in each of the principal directions i of the sub-laminate: $F_{i_{n+1}} = (\{\varepsilon\}^T_{n+1}[\Lambda]_i\{\varepsilon\}_{n+1})^{1/2}$, where $[\Lambda]_i$ is the matrix of coefficients involving the constants K, L, S, T, and U for the appropriate direction i (see Eq. (12)).
3. Evaluate the damage loading function: $f_i = F_{i_{n+1}} - r_{i_n}$, where r_i is a monotonically increasing deformation history parameter defined as $r_{i_n} = \max(F_{i_n}, F_i^{\mathrm{I}})$ in which F_i^{I} is the threshold value for damage initiation in the i direction. Note that the initial value of r_i at time $t = 0$ is F_i^{I}, i.e. $r_{i_0} = F_i^{\mathrm{I}}$.
4. If $f_i < 0$ then $r_{i_{n+1}} = r_{i_n}$ and $\omega_{i_{n+1}} = \omega_{i_n}$. In this case the damage parameters and the elastic constants need not be updated.
5. If $f_i > 0$ then $r_{i_{n+1}} = F_{i_{n+1}}$ and the new damage parameters $\omega_{i_{n+1}}$ are computed using Eq. (8). The corresponding modulus reductions are computed from Eq. (17) and the updated constitutive stiffness tensor $[C]_{n+1}$ is evaluated according to Eq. (23).
6. Compute the stresses that correspond to the current level of strains, $\{\sigma\}_{n+1} = [C]_{n+1}\{\varepsilon\}_{n+1}$.
7. The updated stresses and history parameters are passed on to the other routines in LS-DYNA and the computation marches forward in time based on standard procedures in explicit codes.

3. Material characterization

One of the most difficult tasks associated with applying many of the available CDM models has been the measurement of the material parameters required. Generally, CDM models have used a simple predefined residual stiffness function (e.g. $E/E^0 = (1 - k\omega)$ where it is typically assumed that $k = 1$) in conjunction with a more complex damage growth law (e.g. the Weibull function used by the MLT model). The damage laws are frequently abstract and the means of determining the parameters required are often not clear. In the current approach, the damage growth function has been carefully chosen to be representative of currently available and published experimental observations. Equally, the residual stiffness functions, although perhaps more complex than many other CDM models, are also representative of experimental observations as will be discussed in the next sections.

There are four sets of material parameters that are required by the model. The first set contains standard material properties such as density and initial elastic modulus that are required by all models: elastic, elasto-plastic, and CDM. The second, third, and fourth sets consist of the points that define the damage growth curves (Eq. (8)), the normalized residual stiffness curves (Eq. (17)), and the constants required by the effective strain functions (Eq. (12)) which are specific requirements of the model developed here.

3.1. Elastic and strength constants

The experimental methods for measuring material elastic and strength constants for FRPs are widely accepted, and standard methodologies exist (see, for example, ASTM (2002)). While relatively simple to perform, the complete series of tests required to characterize a given material system are expensive both in terms of time and resources. With over four decades of research in the field of composites there exists an extensive body of published characterization data available for many of the widely used material systems (see for example Tsai (1988)). These data can be supplemented by material suppliers and larger material end-users that frequently have libraries of material characterization data for use in design calculations.

3.2. Residual stiffness functions

The characterization of the effect of damage growth in a laminated composite requires the measurement of the material behaviour under stable crack growth. Traditional testing techniques such as un-notched

coupon tensile tests result in unstable crack growth soon after damage initiation. The measurement of stiffness loss over an appreciable loading range is therefore not possible using these techniques. Experimentally there are two ways to achieve stable crack growth:

- grow the damage very slowly (e.g. cyclic or fatigue loading), or
- grow the damage in a very constrained manner in a test specimen under non-uniform deformation field (e.g. compact tension specimen).

Most literature on the subject concentrates on the first method, fatigue crack growth, as a means of characterizing the susceptibility of composites to subcritical damage growth: initial flaws and in-service damage. As a result little work has been done on damage past saturation of matrix cracking. Typically, the initiation of any substantial fibre damage is considered to be outside the acceptable range of loading.

Some notable examples of fatigue crack growth investigations include the work by Highsmith and Reifsnider (1982), Ogin et al. (1985), Talreja (1985a), and Kress and Stinchcomb (1985), to name but a few. A significant outcome of this body of work was the notion that changes in moduli observed during the fatigue testing of coupons provides a direct quantitative measure of damage (Poursartip et al., 1986; Camponeschi and Stinchcomb, 1982). Therefore, the converse is true, i.e. a physical measure of damage can be used to quantitatively predict changes in modulus. Herein lies the physical basis for the residual stiffness functions presented above in Section 2.5. This relationship between damage and modulus also allows the characterization of modulus loss based on the available body of literature on fatigue damage growth.

As discussed in Section 2.5, the first segment of the residual stiffness curve is most easily characterized by defining the residual stiffness at matrix crack and delamination saturation (R'_E at $\omega = \omega'_m$). The transition point between the two mechanisms, ω^{II}, is a direct consequence of the value of ω'_m and the damage thresholds discussed in Section 3.3 below. A simple mathematical approach that can be used to estimate the stiffness loss at saturation of matrix damage is the ply-discount method.

Implicit in the ply-discount method is the assumption that the crack growth is unconstrained. Results by Talreja (1985a), among others, have shown that ply-discount predictions can either over- or under-predict the stiffness loss due to matrix damage depending on the ply lay-up. In response to this, various analytical methods have been proposed including a modified ply-discount method by Highsmith and Reifsnider (1982), a damage mechanics approach by Talreja (1985a,b), and a more detailed micromechanical analysis by Laws and Brockenbrough (1987). While providing more insight into the effects of changing crack density and crack geometry on stiffness loss, it is unclear if the added complication of these approaches is warranted in the current analysis where only the stiffness loss at saturation of matrix cracking is desired. Although errors of five or ten percent in the prediction of the overall stiffness reduction due to matrix damage may be significant in some applications, results of the application of the model presented here (see Section 5) show that predictions are not very sensitive to such variations in R'_E.

The definition of the level of damage at which the matrix damage saturates, ω'_m, is a consequence of the representation of the damage as the volume or projected area of damage in the sub-laminate. A simple ratio of the net and total cross sectional areas can be used to estimate ω'_m:

$$\omega'_m = 1 - \frac{A_{\mathrm{Net}}}{A_{\mathrm{Total}}} \tag{31}$$

where A_{Total} is the total cross-sectional area and A_{Net} is the cross-sectional area of the remaining load bearing material. The discussion above assumes that damage or cracking in the failed plies at saturation of matrix damage is complete. It also assumes that there is no stacking sequence effect. This is not strictly accurate. A $[0/\pm 45/90]_{n\mathrm{S}}$ lay-up will be more prone to delamination than a $[0/45/90/-45]_{n\mathrm{S}}$, for example. However, the approach provides a first approximation of ω'_m.

While providing guidance on appropriate values for R'_E and ω'_m, the methods described above are intended for cases where experimental results for the particular material and stacking sequence are not available. As mentioned above, the ply-discount method is not a completely accurate predictor of stiffness loss due to damage. Talreja (1985b), for example, obtained experimental results for normalized stiffness reduction as a function of applied stress for a $[90_3/0]_S$ GFRP and a $[45/90/-45/90/45/90/-45/90/90]_S$ CFRP. The experimentally measured normalized stiffness at saturation of matrix cracking was 0.6 for the $[90_3/0]_S$ GFRP and 0.72 for the $[45/90/-45/90/45/90/-45/90/90]_S$ CFRP. Some other examples include the work by Bakis and Stinchcomb (1986) (effect of loading condition on stiffness reduction) and Kress and Stinchcomb (1985) (effect of material lay-up).

In the preceding discussions of stiffness reduction due to matrix cracking, no mention has been made of delamination. While a significant mode of failure in laminated composites, the difficulties associated with modelling delamination in a plane-stress analysis has often lead to the omission of an explicit description of its effect on the material response. In the analyses presented here, delamination and matrix damage have been treated synonymously. All discussion of the effect of matrix damage on stiffness through reduction functions, R_X, applies equally to delamination.

This implicit combination of the intralaminar and interlaminar matrix failure modes is based on work that has shown that the two damage modes generally occur together. There are a few exceptions such as delaminations that grow from a free surface (e.g. the free edge of a plate or a hole) in the absence of intralaminar matrix cracking (Hsu and Herakovich, 1977; O'Brien, 1982) and matrix cracking that can occur in internally pressurised composite cylinders without causing significant delamination (e.g. Hull et al., 1978). In most cases, however, matrix cracking drives delamination between plies of dissimilar lay-up angle, which in turn drive more matrix cracking when the delamination front reaches the fibre direction of the neighbouring ply. Further, work by a number of authors has shown that the in-plane stiffness loss in angle-ply laminates varies linearly with delamination size (Poursartip et al., 1986). Experimental measurements of stiffness reduction due to matrix cracking already include the effects of delamination and, as the reduction is linear with size of damage (i.e. ω), the linear residual stiffness function presented in Eq. (17) is still valid.

3.3. Damage growth functions

Characterization of the two damage growth functions is simply a matter of defining the thresholds for initiation of the two damage modes, matrix cracking/delamination and fibre failure. The other pieces of information required, namely the values for ω'_m and ω'_f ($\omega'_f = 1 - \omega'_m$), have been defined in the discussion of stiffness reduction in Section 3.2.

3.3.1. Mathematical approach

Characterizing the values of the damage thresholds F^{I}, F^{II}, and F^{III} may seem difficult due to the interaction between the normal and shear strains in the damage potential functions (Eq. (12)). However, this task is greatly simplified if one notes that in the case of a uniaxial strain, the damage potential functions simply become a function of the applied strain. From Eq. (25) F^{I}, F^{II}, and F^{III} are the applied uniaxial strains at which each failure mode (matrix cracking/delamination, fibre failure, and final rupture) initiates.

One effect that is not taken into account by such a simple mathematical approach is the constraint offered by neighbouring undamaged plies. The strain at the onset of matrix cracking is observed to increase as the degree of constraint increases (Talreja, 1985a). For example, F^{I} in the 0° ply direction for a $[0/90]_{4S}$ is observed to be higher than the corresponding value for a $[0/90_3]_S$. For other angle-ply laminates the effect of the constraint depends on the lay-up and is by no means intuitive. Talreja (1985a) observed almost no difference between the strain required for initiation of matrix cracking in a $[60/90/-60/90/60/90/-60/90]_S$ and that of an unconstrained 90° ply.

If an increased level of accuracy is desired, one must turn to experimental measurements of the strain at onset of each phase of damage. The same curves for stiffness reduction as a function of applied load used above to estimate R'_E, can also provide information on F^{I} and F^{II}. F^{I}, the strain at onset of matrix cracking, can be evaluated directly from measured matrix crack density as a function of the applied strain (see the results presented by Talreja (1985a) and Highsmith and Reifsnider (1982), for example).

3.3.2. Rupture threshold

The parameter which is the least intuitive is the threshold for rupture, F^{III}. Here one must rely exclusively on experimental data. There is no simple analytical method available for estimating this value as it depends strongly on the lay-up and on interactions between neighbouring plies, both damaged and undamaged. Work by Kongshavn and Poursartip (1999) provides some insight into an experimental technique that can be used to measure this value. Kongshavn and Poursartip grew damage in a composite laminate by loading a pre-notched oversized compact tension (OCT) specimen. The damage zone ahead of the notch was observed to develop in a stable manner as it progressed across the specimen.

The stiffness loss and strain-to-failure of the damaged material in the softening zone were measured by cutting small tensile specimens from the damaged and undamaged zones and loading them to failure. Specimens cut from the undamaged region showed stiffnesses similar to the laminate stiffness and failure strains on the order of the fibre failure strain ($\sim$1.5%). These results would be expected from standard unnotched laminate tensile tests. By contrast, specimens cut from within the damaged zone (process zone ahead of the crack) showed very low stiffness but high strain (nominal) to failure, typically 3–4% for the material investigated. These results are significant because they are much higher than the fibre failure strains. Kongshavn and Poursartip's experimental technique offers a robust and physically meaningful methodology for measuring this characteristic and the results of a statistically significant number of specimens should yield an accurate measure of F^{III}.

3.4. Effective strain functions

As mentioned previously, the selection of the damage potential function presented in Section 2.4 is the least physically based aspect of the model development. As a result, a detailed methodology for characterizing the required parameters (K, L, S, T, and U) is not currently possible. However, it is possible to argue from a purely intuitive point of view what some of the constants in Eq. (12) should be.

4. Post-processing and physical interpretation of damage

The formulation of CODAM3Ds damage model lends itself to interpretation of damage in a manner that is consistent with experimental observations.

Experimental measurements of matrix damage in composite laminates generally come from damage maps generated by pulse-echo ultrasonics (PEUS), C-scan, or other non-destructive measurement techniques, and section micrographs. Fibre damage is usually measured using the deply technique. Careful separation of the individual laminae allows a visual inspection of fibre damage which can then be quantified by measuring the width across which the fibres have been broken and summing them up for each ply. Multiplying the total fibre breakage length by the ply thickness results in quantification of the fibre breakage area (Delfosse et al., 1995).

A method of predicting matrix and fibre damage based on the interpretation of the damage state with reference to the damage growth functions has been incorporated in the model. If the current state of damage, ω, at an integration point in a finite element falls on the first portion of the damage growth function, it can be entirely attributed to matrix cracking and delamination ($\omega = \omega_m$). The relative amount

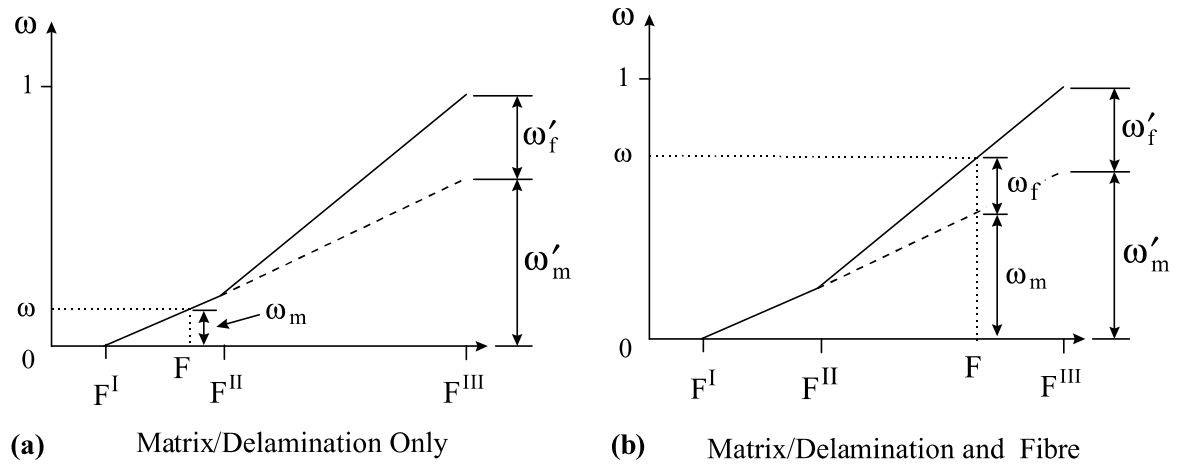

Fig. 8. Portion of damage attributed to matrix cracking/delamination (ω_m) and to fibre breakage (ω_f) for a given damage state (ω).

of matrix cracking is then determined by the proportion of the damage at saturation which is made up of matrix cracks and delaminations, ω'_m in Fig. 8a:

$$\%\ \text{matrix damage} = \frac{\omega_m}{\omega'_m} \times 100\% \tag{32}$$

If the damage state falls on the second segment of the curve, the total damage is made up of a portion of fibre breakage and a portion of matrix damage/delamination. Again, the relative amounts of each can be determined using the damage growth curves as shown in Fig. 8b:

$$\%\ \text{matrix damage} = \frac{\omega_m}{\omega'_m} \times 100\% \tag{33}$$

$$\%\ \text{fibre damage} = \frac{\omega_f}{\omega'_f} = -\frac{\omega - \omega_m}{1 - \omega'_m} \times 100\% \tag{34}$$

The representation of these percentages as an actual total area of damage involves an interpretation of experimental observations of the area of matrix cracking and fibre breakage in a sub-laminate at saturation of damage. For example, at the saturation of damage in a four ply sub-laminate the staircase or helical pattern of delamination and associated matrix cracking results in a total area of matrix cracking approximately equal to the in-plane area of the sub-laminate.

Consider an example. Assume that each integration point represents a sub-laminate, and that the planar area of an element is 10 mm^2. Further assume that the lay-up is quasi-isotropic such that the area of matrix damage at saturation in a sub-laminate is also equal to 10 mm^2. If the percentage of matrix damage for an integration point (i.e. sub-laminate) were predicted to be 84% then the area of matrix damage in that sub-laminate would be calculated to be 8.4 mm^2. These matrix damage areas can then be summed over the entire finite element mesh to give a prediction of the total matrix damage area.

While the same calculations apply to fibre damage, the area of fibre breakage associated with saturation of damage in a sub-laminate is not as simple to define. Experimental evidence shows that the amount of fibre damage is not simply a function of the lay-up. Not only does fibre damage tend to be more localized

than matrix damage but the material system (e.g. brittle versus tough matrix) plays a role as well (Delfosse et al., 1995). For a quasi-isotropic sub-laminate, a reasonable first approximation may be four times the cross sectional area of a ply, or simply the cross sectional area of the sub-laminate, times the fibre volume fraction (i.e. roughly the total cross-sectional area of fibres).

5. Numerical application

Typical structural problems involve dynamic loading and detailed predictions of the various damage modes are of interest. To investigate the application of the model to these types of problems, an extensive investigation of out-of-plane impact loading of composite test coupons by Delfosse (1994) has been used as the basis for a case study, the results of which are summarized below. Further synthesis and analysis of the experimental data has been presented in Delfosse et al. (1995) and Delfosse and Poursartip (1995) all of which have been used to guide the application of the model and the discussion of the numerical predictions. The experimental work investigates the influence of a number of material and target related parameters (e.g. target thickness, material, boundary effects, and indenter shape) on the normal impact response of polymeric composites.

5.1. Experimental set-up

The target geometry used predominantly in the experimental investigation is that of a 101.6 mm by 152.4 mm (4 inch by 6 inch) coupon clamped on to an aluminium backing plate with a 76.2 mm by 127.0 mm (3 inch by 5 inch) rectangular opening. The plate geometry is consistent with the Boeing (1988) and SACMA (1988) compression after impact (CAI) standards. In all the test results discussed below, a 25.4 mm (1.0 inch) diameter hemispherical tipped hardened steel indenter was used. The gas gun projectile weighed 0.314 kg and was launched at velocities up to 50 m/s. The low velocity, high mass tests include results from two drop-weight apparatuses with indenter masses of 6.141 and 6.330 kg.

In addition to the force and displacement-time histories, detailed post-test damage characterizations were carried out by Delfosse and Poursartip (1995). Quantitative measurements of matrix damage, characterized by delaminations, and of fibre breakage were made using PEUS and C-scan images, section micrographs and deplies.

5.2. Objective

The goal of the numerical case study was to quantitatively predict the various experimental measurements made during the test series. These comparisons include force and displacement-time histories and total fibre and matrix damage, size of fibre and matrix damage zones, and energy loss, all as a function of available energy. For the purposes of the current study, two parameters were selected as variables for evaluating the performance of the CODAM3Ds model: target material and available energy. Of particular interest to the current investigation are the drop-weight and gas gun tests performed on CFRP systems: T800H/3900-2 and IM6/937 with quasi-isotropic stacking sequences of $[45/90/-45/0]_{3S}$ and $[45/0/-45/90]_{3S}$, respectively. While both materials have similar elastic properties, the 937 resin used in the latter is more brittle providing a contrast with the tougher 3900-2 matrix system. If the differences in the material model input can be argued from a physical point of view, or from experimental observations (i.e. not using calibration constants) then the predictive capability of the model can be used with a greater degree of confidence.

Table 1
Characterization data for the T800H/3900-2 plates

Lamina		Sub-laminate [45/90/−45/0]		Units
Parameter	Value	Parameter	Value	
ρ	1543	ρ	1543	kg/m^3
E_1	129.1	E_x	48.37	GPa
E_2	7.45	E_y	48.37	GPa
G_{12}	3.52	G_{xy}	18.36	GPa
v_{12}	0.33	v_{xy}	0.320	
t_{ply}	0.194	t_{sublam}	0.775	mm
X_{t}	2089	N/A	–	MPa
X_{c}	1482	N/A	–	MPa
Y_{t}	79	N/A	–	MPa
Y_{c}	231	N/A	–	MPa
S_{c}	133	N/A	–	MPa
m	10	N/A	–	

Elastic constants are from Ilcewicz (1992), the strength constants are from Straznicky et al. (1993), and the MLT constant, m, is from Williams and Vaziri (1995, 2001).

5.3. Material characterization

Lamina elastic properties for the T800H/3900-2 CFRP are shown in Table 1. The effective sub-laminate properties were obtained using classical laminate plate theory (CLPT). Also shown in Table 1 are the lamina strength properties required by the Chang and Chang (1987) and the Matzenmiller et al. (1995) models, which are the two other constitutive models used here for comparison purposes. The Weibull shape parameter, m, required by the MLT model was calibrated in a previous investigation by Williams and Vaziri (1995, 2001).

The constants used to characterize the damage growth and residual stiffness functions of the CODAM3Ds model are summarized in Table 2. Simple mathematical analyses such as the ply discount method have been used to derive most of the values. Where possible, published experimental data has been used to guide the selection of these parameters. The experimental work by Kress and Stinchcomb (1985) and Poursartip et al. (1986), for example, provide the background experiments for the selection of the residual stiffness constants while Camponeschi and Stinchcomb (1982) and O'Brien and Reifsnider (1981) guided selection of the residual shear modulus at matrix damage saturation.

Table 2
CODAM3Ds damage model characterization for T800H/3900-2

Parameter	Value		Paramet	Value	
	Tensile	Compressive		Tensile	Compressive
ω'_m	0.800	0.800	K_x	1.000	1.200
R'_E	0.650	0.650	K_y	1.333	1.400
R'_G	0.650	0.650	L_x	1.333	1.400
F^{I}	0.010		L_y	1.000	1.200
F^{II}	0.016		$S_x = S_y$	4.000	
F^{III}	0.040		$T_x = T_y$	1.000	
ω_E^{II}	0.160		$U_x = U_y$	1.000	
ω_G^{II}	0.160				
E^{II}	0.930	0.930			
G^{II}	0.930	0.930			

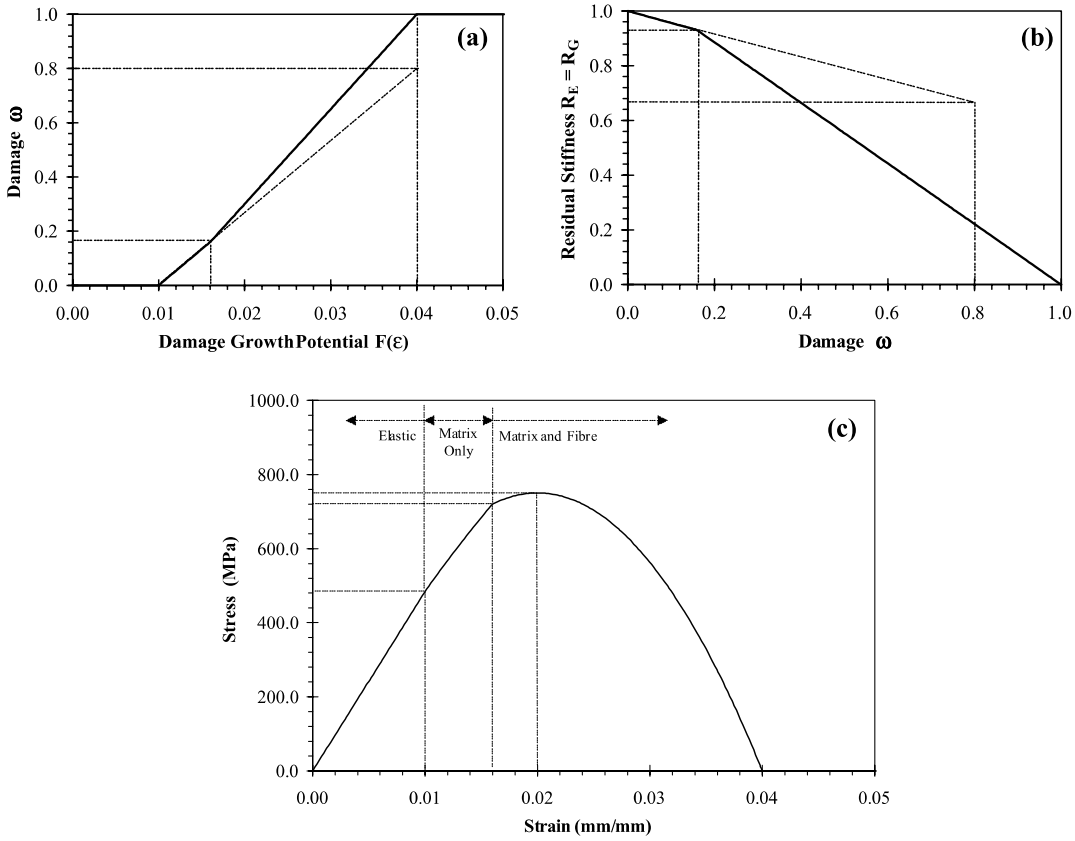

Fig. 9. (a) Damage growth function, (b) residual stiffness function, and (c) predicted one-dimensional stress–strain response for the T800H/3900-2 material.

The damage growth and residual stiffness functions defined by the parameters in Table 2 are shown in Fig. 9a and b, respectively, while the resulting 1D stress–strain response for the CODAM model of T800H/3900-2 is shown in Fig. 9c. A detailed description of the procedure used to arrive at the parameters listed in Table 2 is presented in Appendix A.

5.4. FEM model

The test coupon is modelled as a simply supported 76.2 mm by 127 mm (3 inch by 5 inch) plate. The hardness of the steel and the relative stiffness of the indenter compared to the through-thickness stiffness of the composite plates also make the assumption of a non-deformable indenter (modelled as a rigid material) reasonable. As a result, only the profile of the indenter has been included in the FEM model (see Fig. 10). Four node quadrilateral Mindlin-type shell elements (developed by Belytschko et al. (1984)) were used throughout the model. For the computations using the CODAM3Ds model, the symmetry of the problem and the in-plane isotropy of the material would have allowed the use of two-fold symmetry (quarter plate symmetry) to reduce the size of the model. However, since two other lamina-based composite damage models were used to provide comparisons with the existing capabilities of LS-DYNA, a full spatial discretization was required. Twelve integration points were used through the thickness, two per sub-laminate.

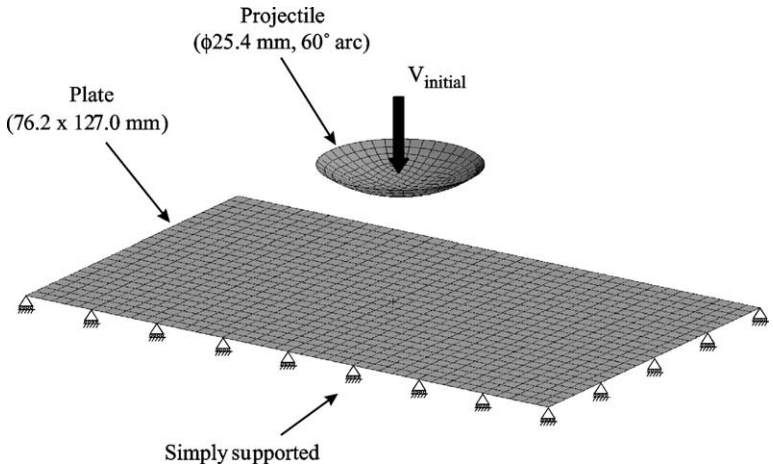

Fig. 10. Exploded view of the FEM model of the CAI standard impact specimen with the assembled mesh. The target mesh consists of 960 uniform elements of size 3.175 mm × 3.175 mm.

A minimum of six could have been used, one for each $[0/45/90/-45]$ sub-laminate. However, the problem involves a significant amount of bending deformation and thus the additional integration points for capturing the through-thickness strain gradients is warranted. The other lamina-based constitutive models require the use of 24 integration points (one per ply) through the thickness.

Hourglass control was achieved using the standard LS-DYNA viscous method with the default coefficients. The default hourglass control parameters were also found to be sufficient to avoid zero energy modes of deformation. Contact between the indenter and plate was modelled using the penalty stiffness method incorporated in LS-DYNA.

A uniform square mesh was selected for the composite plate so as to preserve an unbiased damage propagation path. In recognition of the inherent mesh sensitivity of strain-softening constitutive models (e.g. Bazant and Cedolin, 1991; and Belytschko et al., 1986) the element size effect is treated using the crack band approach proposed by Bazant and Oh (1983). Accordingly, the amount of energy dissipation during the damage process, or energy release rate $\mathscr{G}_f$ is taken to be equal to the energy density (area under the uniaxial stress–strain curve) times the characteristic length h of the element. This quantity, which can be thought of as the energy consumed in the formation and propagation of damage per unit area in a representative volume element of material is a material constant determined from tests. To maintain $\mathscr{G}_f$ constant and therefore retain the objectivity of the numerical modelling, the slope of the softening curve (post-peak branch of the stress–strain curve) would have to vary with the element size h. The smaller the element size, the shallower (flatter) the softening curve would be. Therefore, for an element that is smaller than a characteristic size (typically equal to the size of the fracture process zone) a relatively large strain would be required to completely exhaust its load carrying capacity. The finite element mesh for the composite plate selected in the current study consists of 960 square shell elements with $h = 3.175$ mm. As discussed in Appendix A, this element size is consistent with the height of the process zone and results in an energy release rate that is comparable with the expected values reported in the literature. A rigid material model with the elastic properties of steel (density $\rho = 7810$ kg/m^3, $E = 208.5$ GPa, and $\nu = 0.33$) was applied to the indenter mesh. The elastic modulus and Poisson's ratio are required by the contact algorithm to predict an appropriate contact stiffness. The use of a simple shell representation of the indenter does not provide the correct kinematic properties because the mass of the shell structure is significantly lower than that of the actual projectile. To compensate for this, a lumped mass with an appropriate value was associated with the central node of the indenter mesh.

Two sets of numerical analyses were carried out for each velocity range. The first set consisted of tests at velocities corresponding to impact energies of 5–60 J of energy, in increments of 5 J. Additional runs at 12, 17, and 22 J were used to provide more resolution in the results near the onset of damage, identified as 18 J for matrix/delamination initiation and 22 J for fibre breakage from the experimental results (Delfosse and Poursartip, 1995). The second set of runs corresponded to the energy levels used in the experimental low and high mass tests.

5.5. Results

5.5.1. Quantitative damage measures

Fig. 11a shows the predictions of total matrix damage in the form of delamination size, as a function of incident or available energy while Fig. 11b shows fibre breakage area as a function of incident energy. In both cases the plots demonstrate the excellent correlation between the FEM results and the experimental observations of Delfosse and Poursartip (1995). The quasi-static tests were performed using a hydraulically actuated MTS load frame. The geometry of the indenter and test fixture were identical to that used in the impact tests. The energy in Fig. 11 is the available energy calculated from the quasi-static force–displacement curve. While the predictions are very good, especially given the simplifying assumptions that have been made in the material characterization, there are deviations from the observed trends. For example, the prediction of delamination damage area shown in Fig. 11a is good for impact energies over 20 J but below that level the FEM model predicts damage where none was observed experimentally. Damage initiation is shown to occur at just 5 J, much lower than the measured 18 J. Even damage histories for a single 60 J impact show the same trend although, interestingly, the initial jump in damage occurs earlier in the high mass impact than in the low mass event. The same over-prediction of damage at energies less than 20 J is observed in Fig. 11b. Numerically, fibre damage appears to be closely coupled to delamination damage. This could possibly result from too low a value for F^{II} but if the interpretation of the threshold for fibre breakage is to be linked with the strain-to-failure of the fibre, values over 1.7% or 1.8% are unreasonable. Rather, the source of the discrepancy can be traced back to the inherent link between the fibre and matrix damage in the damage growth function. The damage growth functions used for the matrix and fibre damage are the same. As a result the model predicts that fibre damage shows the same sensitivity as matrix damage to off-axis strains. In reality, fibre damage is primarily driven by strains in the fibre direction. As a

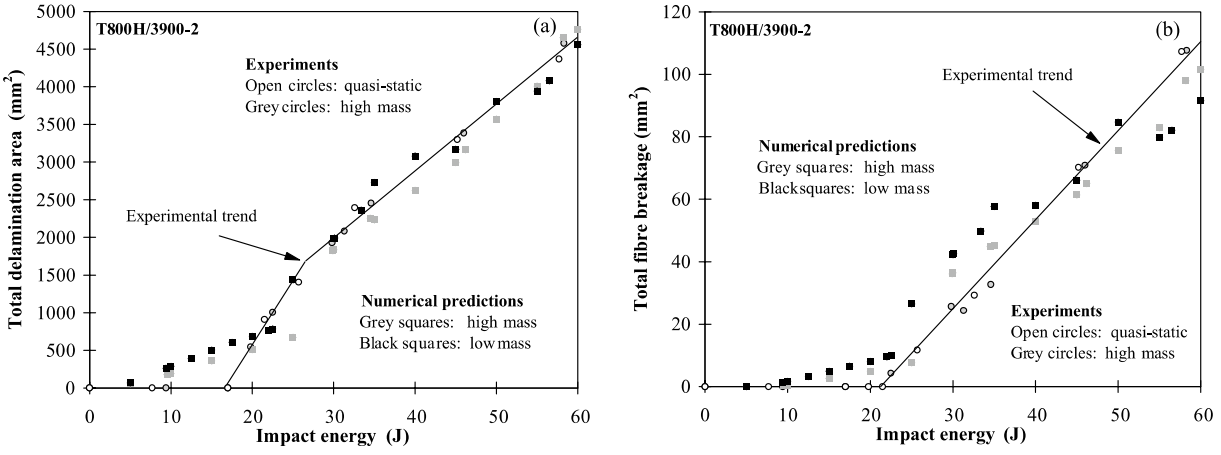

Fig. 11. Comparison of experimentally measured and predicted (a) total delamination area and (b) total fibre breakage area as a function of incident energy for a $[45/90/-45/0]_{3S}$ T800H/3900-2 CFRP plate.

result, the model over-predicts the fibre damage at low strains where the added effect of the off-axis strains can push the damage potential over the limit for fibre failure. Matrix damage grows with the stiffness loss that results from this fibre damage. The end result is too much damage predicted at lower strains. The error is relatively small though, and the experimental measurement could have overlooked some damage as well, as one would expect at least some very minor damage to grow right from the load application.

The drop in fibre breakage area above 50 J of impact energy is associated with the localization of the damage growth due to the complete loss of stiffness of the elements directly under the indenter (see also Section 5.5.2). This localization of the damage reduces the driving force for further damage in the neighbouring elements. Note that the localization does not affect the prediction of the delamination area as much although the prediction of delamination area also falls below the experimental measurements above 50 J. Saturation of matrix cracking occurs before the complete stiffness loss of the element and is associated with only a partial decrease in the load carrying capability of the material allowing continued load transfer, and hence damage growth, in neighbouring elements. If the comparison were to have been continued to even higher energy levels one would expect the effect to become more significant on the delamination damage prediction.

5.5.2. Qualitative damage predictions

Fig. 12 compares the predictions of projected matrix damage/delamination size (ω_m/ω'_m in Eq. (32)) to C-scan images of delamination growth for the low mass impact events (i.e. gas gun tests). Both sets of images (numerical and C-scan) are to the same scale. The C-scans were taken across the width of the specimens so the whole plate is not visible. The box drawn around the numerical results highlights the location of the plate boundaries relative to the part of the plate modelled (i.e. a 127.0 mm by 76.2 mm simply supported plate). The low levels of damage predicted at the mesh boundaries at higher energy levels (e.g. 33.4 and 56.4 J in Fig. 12) are caused by local through-thickness shear strains, an effect of the boundary condition applied at the edge of the plate. The qualitative comparisons of the size of the predicted and measured damage zones are excellent over the whole range of impact energy levels. It is interesting to note that even the predicted localization of the damage growth along the length of the specimens is not unrealistic. Although, numerically this localization is confined to a region of only one or two elements wide, the C-scan images show the same preferred direction in the damage growth at impact energies of over 30 J. The asymmetry in the predictions at higher energy levels is a result of localization of the damage mentioned in the previous section. As elements fail (i.e. $\omega = 1$), the redistribution of the loading to neighbouring elements may no longer be symmetric. This can drive more damage in one direction resulting in an asymmetry of the predicted damage pattern. At low impact energies, none of the elements fail completely and the symmetry of the damage growth is preserved.

5.5.3. Force-time histories

Examples of the predicted force-time histories for two of the high mass (drop-weight) experiments are shown in Figs. 13 and 14. To assess the performance of the CODAM3Ds model against current composite models in the LS-DYNA code, two other material models have been used to analyse the same problem. MAT22 in LS-DYNA is a composite failure model based on the work of Chang and Chang (1987) and is one of the most widely used composite models in LS-DYNA. Failure is predicted in a number of modes including matrix cracking and fibre splitting using modifications of the criteria proposed by Hashin (1980). The second model is based on the CDM approach developed by Matzenmiller et al. (1995) (MLT model), which was implemented as a user material model in LS-DYNA (Williams and Vaziri, 1995, 2001). In both cases, the effect of the damage on the laminate response is modelled on a lamina-by-lamina level (an integration point per lamina).

Fig. 13 shows results for a high mass 34.5 J impact. The MLT and CODAM3Ds models exhibit very good agreement with the experimental measurements. While the MLT model slightly over-predicts the peak

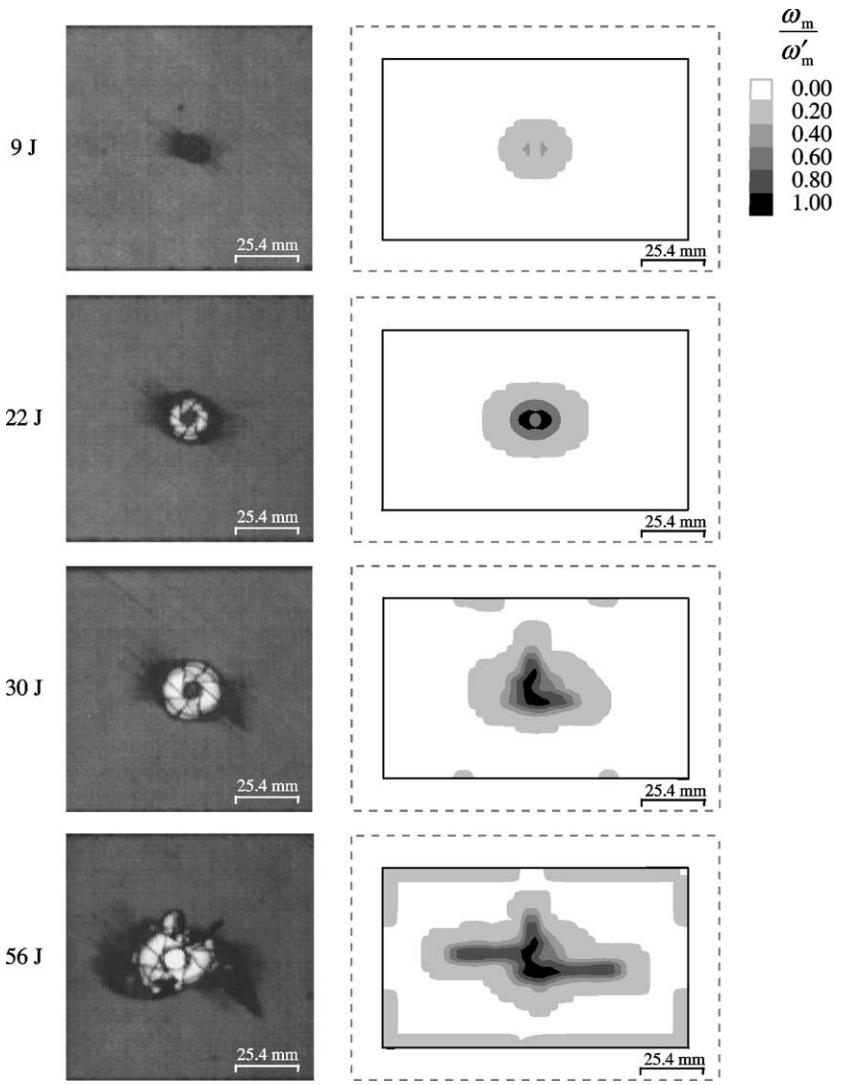

Fig. 12. Comparison of predicted projected matrix/delamination damage and experimental C-scan images for low mass impact events on a $[45/90/-45/0]_{3S}$ T800H/3900-2 CFRP plate. Results presented are for (a) 9.4 J ($v = 7.74$ m/s, $m = 314$ g), (b) 22.0 J ($v = 11.84$ m/s, $m = 314$ g), (c) 33.4 J ($v = 14.59$ m/s, $m = 314$ g), and (d) 56.4 J ($v = 18.97$ m/s, $m = 314$ g) impacts.

forces, the CODAM predictions show a sudden drop in force (i.e. jump in damage growth leading to an abrupt loss in plate stiffness) of a larger magnitude than that observed experimentally. Note, however, that the time and hence projectile displacement at the onset of substantial damage growth is very close to that observed experimentally. This over-prediction of the stiffness loss in the plate also leads to a slight over-prediction of the duration of the event. It is important to note that the MLT results were the final product of an extensive parametric study used to arrive at a reasonable value for the m parameter in the Weibull function for damage (Williams and Vaziri, 2001). The CODAM results required no such curve fitting exercise. In marked contrast to the MLT and CODAM3Ds results, the Chang and Chang failure model

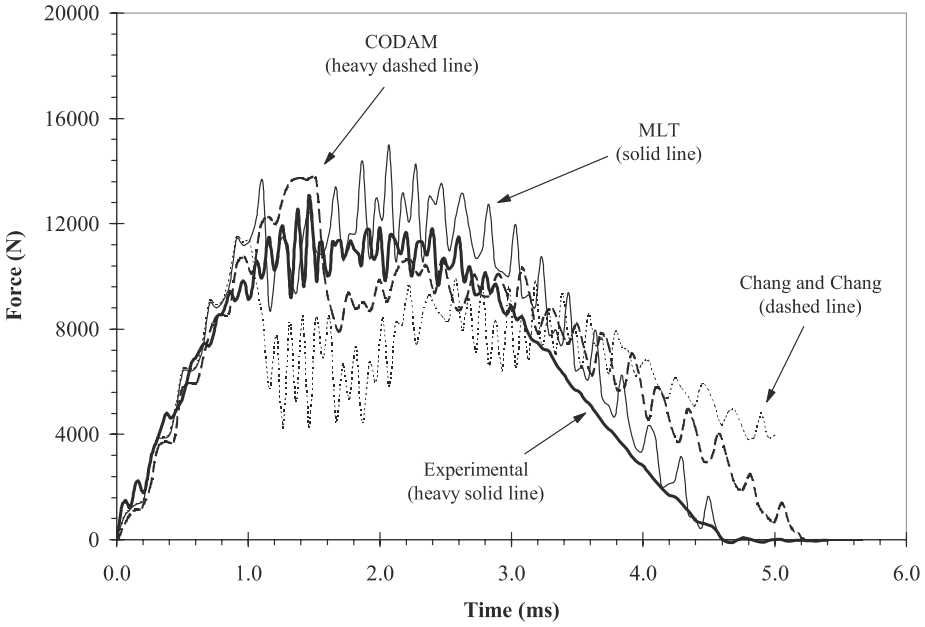

Fig. 13. Comparison of predicted and measured force-time histories for a high mass 34.5 J event on a $[45/90/-45/0]_{3S}$ T800H/3900-2 CFRP plate.

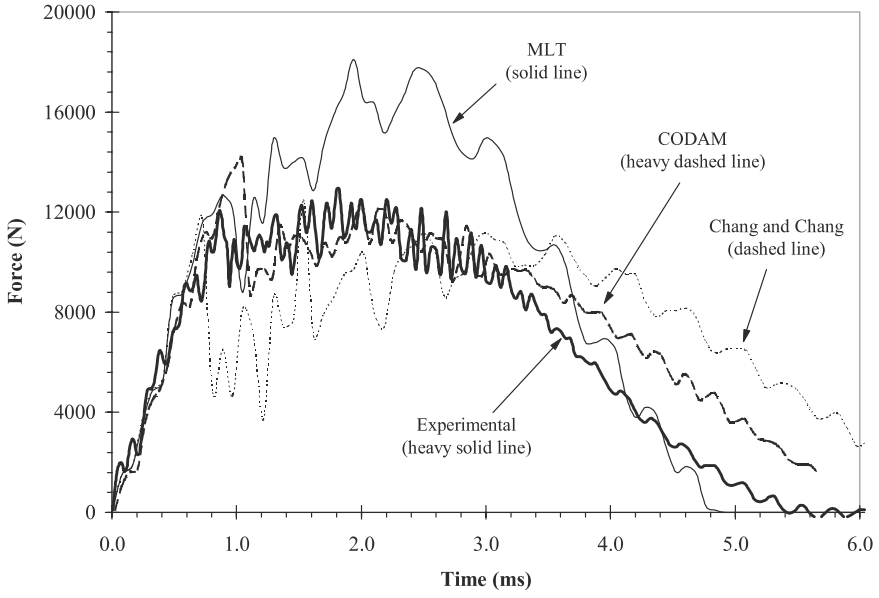

Fig. 14. Comparison of predicted and measured force-time histories for a high mass 58.2 J event on a $[45/90/-45/0]_{3S}$ T800H/3900-2 CFRP plate.

significantly under-predicts the peak force and the initiation point for significant stiffness loss. The net result being a large over-prediction of the duration of impact event.

Fig. 14 shows the same series of results (experimental, CODAM3Ds, MLT, and Chang and Chang) for a higher energy impact at 58.2 J. The CODAM results again compare extremely well with the experimental observations. Here the same sudden drop in stiffness is observed. This time, its position seems to indicate a delay in the onset of damage growth compared to the experiments. The MLT results are extremely poor in this case. The same constant (i.e. $m = 10$) and hence the same shape for the strain-softening curve has been used but the peak force is over-predicted by 50%. Williams and Vaziri (2001) showed that it was necessary to change (increase) the Weibull shape factor, m, as the energy level of the impact increased in order to achieve good agreement with the experimental results. The CODAM3Ds model continued to show good agreement up to energy levels of 84 J (Williams, 1998) without needing to change the characterization. Finally, it is worth noting that the Chang and Chang model still fails to capture the characteristics of the measured force-time history.

5.5.4. Effect of material characterization

Fig. 15 shows the predicted and measured matrix damage growth as a function of incident energy and compares the results of the T800H/39000-2 system with those of IM6/937. Both are CFRPs but the 937 resin is a more brittle matrix system. Note that the present numerical model accurately captures the distinct trends associated with the two materials. This is most significant because the only difference between the two numerical models, apart from the elastic material properties, is the characterization of the damage growth functions. The residual stiffness functions are, to a reasonable approximation, only a function of the material lay-up and the difference between the $[45/90/-45/0]$ T800H/3900-2 and the $[0/45/-45/90]$ IM6/937 is not significant in this respect. However, a difference in the damage growth functions is expected. The IM6 and T800 fibres have similar values of strain-to-failure and only the properties dominated by the matrix response will change. These include the onset of matrix damage (characterized by F^{I}) and the rupture threshold (F^{III}). Guided by published values for the onset of matrix cracking strain and for the rupture strain (e.g. the work of Kongshavn and Poursartip, 1999), the damage growth functions for the T800H/3900-2 material were modified to represent the behaviour of the IM6/937 material system. A more detailed

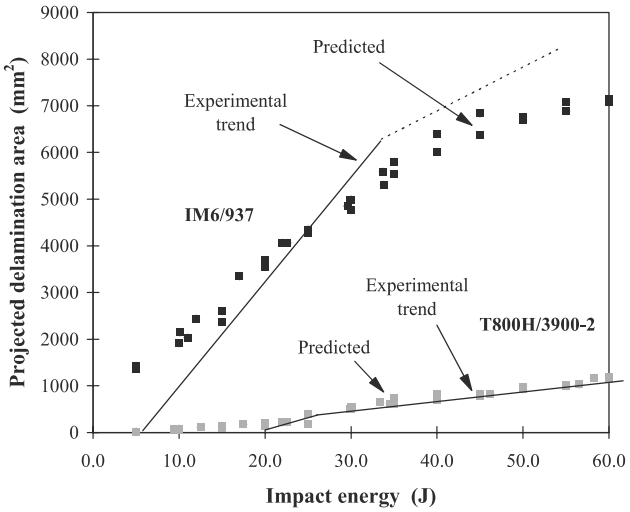

Fig. 15. Projected delamination size as a function of impact energy showing the difference in damage zone size between the brittle (IM6/937) and tough (T800H/3900-2) CFRP systems. Numerical predictions for each system are also shown. The FEM data shown combine the high and low mass results. Note that only the trends of the experimental data are shown.

discussion of the parameters used for the IM6/937 and of the comparison between the brittle and tough matrix composites results is presented in Williams (1998) and is the subject of an upcoming publication.

6. Summary and conclusions

A mathematical model has been developed to predict damage growth and its effects on the response of laminated FRP composites. The formulation is based on the sub-laminate response, in recognition of the fact that the laminate response is driven not only by the lamina properties but also by the ply interactions through the stacking sequence and damage growth (i.e. it is a system response). The resulting application of CDM model at the sub-laminate level within the FEM framework leads to a formulation that is both physically meaningful and mathematically simple.

Throughout the model development, the implications of experimental observations of damage growth and of the effects of damage on the material response have been used to derive the mathematical formulation. The model is based on a two-phase material response, the first dominated by matrix cracking and delamination and the second by combined matrix and fibre damage growth. The bilinear damage growth and residual stiffness functions used to describe this behaviour have been constructed based on a simple interpretation of available experimental observations of damage growth and associated degradation in material properties.

Methodologies for determining the material constants required by the model have also been discussed. The most significant aspect of the methodologies is that they are based entirely on a physical interpretation of damage in laminated FRPs. Most properties can be gathered from the literature provided a well-established base of research exists for the desired composite system. Where experimental data is not available, simple analytical techniques have been proposed to provide order-of-magnitude estimates of many of the model input parameters.

One of the main features of this model, which makes it advantageous over other CDM based models is that it lends itself to physically meaningful predictions of damage size and distribution that can be compared directly with experimental measurements. The brief overview presented in this paper of some of the results from a particular case study, namely the prediction of the response of a laminated plate to normal impacts, clearly shows the capabilities of the model. The results show that simple physical reasoning based almost entirely on widely available, published material characterization data, which in turn is based on relatively simple standard test schemes, can be successfully used to define the input parameters required to characterize the model.

Acknowledgements

The authors gratefully acknowledge the financial support provided by the Natural Sciences and Engineering Research Council of Canada and the Defence R&D Canada (DRDC)—Valcartier with Dr. Dennis Nandlall as the Scientific Authority. We would also like to acknowledge many interesting discussions and influences from our colleagues at DRDC, The Boeing Company, and elsewhere.

Appendix A. Material characterization of T800H/3900-2 for the CODAM model

This appendix describes in more detail the procedure used to characterize the properties required by the CODAM constitutive model. As discussed in Section 5.3, CLPT was used to derive the effective sublaminate elastic properties for the T800H/3900-2 CFRP shown in Table 1. The constants used to characterize the damage growth and residual stiffness functions of the CODAM model are summarized in Table 2. As

the material has a quasi-isotropic lay-up, the in-plane constants for both directions, x and y, are the same. The only exceptions are the scale factors K_i and L_i, on ε_x and ε_y respectively, where $K_{1c,t} = L_{2c,t}$ and $K_{2c,t} = L_{1c,t}$. To simplify the discussion of the derivation of these material constants, let us associate the x- and y-directions with the 0° and 90° ply directions, respectively.

As was discussed in Section 2.7, the response predicted by the 1D CODAM model is independent of ω'_m. As this remains to be proven in the multidimensional implementation of the model, an appropriate value must be selected. Using a simple volumetric analysis and making the assumption that the matrix cracking at saturation associated with a given direction in the laminate will result in complete matrix cracking of all off-axis plies (i.e. the ±45° and 90° plies, for the x-direction), one obtains:

$$\omega'_m = \frac{A_{\text{damaged}}}{A_{\text{total}}} = \frac{n_{-45} + n_{45} + n_{90}}{n_0 + n_{-45} + n_{45} + n_{90}} = \frac{3}{4} \cong 0.8$$

The residual stiffness at saturation of matrix cracking, R'_E, is estimated using the ply-discount method. The same assumptions noted above for ω'_m apply here. Further, in the application of the model a significant amount of delamination is expected and so it is possible to assume that the off-axis plies do not contribute to the stiffness once a significant amount of matrix cracking has been induced in the material (i.e. a completely decoupled response). Under these conditions, according to the ply-discount method, the damaged stiffness of the laminate is $E_{\text{lam}} = 129.1/4 = 32.28$ GPa and since $E^0_{\text{lam}} = 48.37$ GPa (Table 1), the residual stiffness becomes $R'_E = E_{\text{lam}}/E^0_{\text{lam}} = 0.67 \cong 0.65$.

Depending on the assumptions made, the ply-discount method can give a wide range of predictions from as low as 0.67 (given the simplifications made above) to as high as 0.89 (a completely coupled response with perfect bonding between the plies such that the ±45° plies continue to contribute to the stiffness). To substantiate the selection of R'_E we must turn to the literature. Experimental work by Kress and Stinchcomb (1985) on fatigue damage growth in T300/5208 CFRP $([0/45/90/-45])_{4S}$ laminates shows stiffness reduction factors as high as 40%. Lafarie-Frenot and Riviere (1988) also show stiffness reductions on the order of 30–40% for quasi-isotropic CFRP lay-ups as do Poursartip et al. (1986). Based on these observations, the ply-discount prediction of $R'_E = 0.65$ is reasonable. Bakis and Stinchcomb (1986) observed that, under fatigue loading, the stiffness reduction in tension was less than that in compression in a quasi-isotropic T300/5208 CFRP with the residual compressive modulus being closer to 75%. However, in the current analysis the difference between tensile and compressive stiffness loss has been ignored.

Using the same assumptions, the ply-discount method predicts a residual stiffness of 0.05 for R'_G, the characterization constant which is required to determine G^{II}. This is clearly unreasonable and again we must turn to the literature for guidance. Data on shear modulus reduction due to damage is much less common than the published work available on the direct elastic modulus E. O'Brien and Reifsnider (1981) noted reductions in G_{xy} of 13–14% in fatigue loaded $[0/90/\pm 45]_S$ boron/epoxy laminates compared to 15–16% in E_x in the same tests. However, Camponeschi and Stinchcomb (1982) observed that the reduction in G_{xy} was almost twice that of E_x in $[0/90/\pm 45]_S$ CFRP laminates. They also concluded that a stacking sequence that avoids ±45° sequences (e.g. the T800H/3900-2 $[0/45/90/-45]_{3S}$ studied here) would be less susceptible to a reduction in G_{xy}. Although this data does not yield a precise value to be used for R'_G, the assumption that $R'_G \cong R'_E$ seems reasonable as a first approximation.

Appropriate values for most of the scaling constants on the strain terms in the damage growth potential functions, F_x and F_y (Eq. (12)), can be argued from intuition. For example, K_{xt} and L_{yt} should be 1 as ε_x and ε_y are the primary drivers of damage in the x- and y-directions respectively. However, appropriate values for K_{yt} and L_{xt} are less obvious. While the effect of ε_y on damage in the x-direction will obviously be less than that of ε_x, the transverse strain still contributes through the ±45° plies and to a lesser extent through cracking induced in the 90° plies of a $[45/90/-45/0]_S$ lay-up. A value of $L_{xt} = 1$ is too low while $L_{xt} = 2$ (i.e. a contribution of $0.5\varepsilon_y$ to ω_x) is too high. Lacking a more physical argument than the one presented here, L_{xt} (and K_{yt} by the same argument) is set to 4/3 (i.e. a contribution of $0.75\varepsilon_y$ to ω_x). The thresholds for

damage growth in compression are generally higher than those in tension (i.e. higher compressive strengths) and values of $K_{xc} = L_{yc} = 1.2$ and $K_{yc} = L_{xc} = 1.4$ are used to reflect this.

The out-of-plane shear actions are assumed to have a secondary effect on damage growth and so T_x and U_x (and T_y and U_y by symmetry) are set to 1. The final parameters, S_x and S_y are more difficult to choose. The degradation of the in-plane shear modulus is expected to result in large shear strains. As a result, a low value for S could cause an instability in the predicted damage growth. On the other hand, in-plane shear certainly plays a role in damage growth and removing γ_{xy} from the damage growth potential functions would be an over-simplification. Results of initial runs of the CODAM model in the plate impact problem supported these observations. A value of $S = 1$ resulted in much too strong a sensitivity to shear stiffness reduction. A value of $S = 4$ was found to be a more reasonable choice. As noted before in Section 2.4, the damage growth potential functions are the least physical component of the model and are the subject of current research. However, this does not affect the validity of the approach.

The thresholds F^{I},F^{II}, and F^{III} are associated with the strain states at the onset of matrix cracking and delamination, fibre breakage, and rupture respectively. Typically, a strain of 0.5–0.7% is associated with first ply failure in unidirectional test coupons of CFRP laminates. Here a value of 1% has been assumed with $F^{\mathrm{I}} = 0.01$. F^{II} is the threshold for fibre failure. Again, in uniaxial tensile tests, fibre failure strains of approximately 1.2–1.7% are observed for typical CFRP materials. The failure strain of T800H fibres as measured from a tensile test on a unidirectional lamina is reported to be 1.6% and therefore F^{II} has been set to 0.016.

Work by Kongshavn and Poursartip (1999) demonstrated rupture strains as high as 3% for material extracted from the process zone (softened material) ahead of the crack tip in T300H/F593 CFRP laminates. The F593 epoxy matrix is considered to be brittle and it is assumed here that in a material with a tougher matrix, such as the 3900-2, it may be possible to achieve stable damage growth at even higher strains.

Lacking any more substantial data on which to base F^{III}, a value of 0.04 was chosen for the T800H/3900-2 material.

Having set ω'_m and F^{I},F^{II}, and F^{III}, ω^{II} can be determined from Eq. (7):

$$\omega^{\mathrm{II}} = \omega'_m\left(\frac{F^{\mathrm{II}} - F^{\mathrm{I}}}{F^{\mathrm{III}} - F^{\mathrm{I}}}\right) = 0.8\left(\frac{0.016 - 0.010}{0.040 - 0.010}\right) = 0.16$$

And given ω'_m, R'_E, G'_m, and ω^{II} we can apply Eq. (15) to determine E^{II} and G^{II}:

$$E^{\mathrm{II}} = G^{\mathrm{II}} = 1 - (1 - R'_E)\frac{\omega_E^{\mathrm{II}}}{\omega'_m} = 1 - (1 - 0.65) = 0.93$$

From Eq. (6) we can assume that $\omega_G^{\mathrm{II}} = \omega_E^{\mathrm{II}}$. In the limiting case of $\omega_x = \omega_E^{\mathrm{II}}$ at onset of fibre breakage and with $\omega_y = 0$, $\omega_S = \omega_E^{\mathrm{II}}$ but $\omega_S = \omega_G^{\mathrm{II}}$ at the onset of fibre breakage and therefore $\omega_G^{\mathrm{II}} = \omega_E^{\mathrm{II}}$. And so, with $R'_E = R'_G$, $G^{\mathrm{II}} = E^{\mathrm{II}} = 0.93$. Note that the assumption that $\omega_G^{\mathrm{II}} = \omega_E^{\mathrm{II}}$ holds for cases where either $\omega_x = 0$ or $\omega_y = 0$, and for $\omega_x = \omega_y$ but is not true for any general damage state.

The damage growth and residual stiffness functions defined by the parameters derived above are shown in Figs. 9a and b, respectively, while the predicted 1D stress–strain response for the CODAM model of T800H/3900-2 is shown in Fig. 9c.

While the initiation of damage may depend on the operative stresses (or strains), from the strictly physical viewpoint the actual formation of damage requires a certain amount of energy, namely the fracture energy. Regardless of the choice of mesh, which is a subjective aspect of numerical analyses, the overall energy dissipation due to damage must remain constant. Otherwise, the results of the numerical solution will not be objective. According to the crack band theory developed by Bazant and Oh (1983) to remedy this problem, for an element that is representative of the characteristic process zone size, the product of the

area under the uniaxial stress–strain curve and the element size corresponds to a fracture energy, $\mathscr{G}_f$ that is a material constant.

In our case the area under the uniaxial stress–strain curve in the post-damage region (corresponding to damage phases 1 and 2 in Fig. 9c) works out to be 17.5 MJ/m^3. Also, the experimental study conducted by Kongshavn and Poursartip (1999) on overheight compact tension specimens of T300H/F593 CFRP material system revealed that the height of the process zone was approximately 5 mm. In a finite element study of such a problem (Williams et al., 1999) one would use an element size of at least 2.5 mm (on either side of the notch) in order to cover the process zone. In the current study we are dealing with a tougher CFRP system where a slightly wider process zone would be expected. Therefore we have chosen a square element size of 3.175 mm (corresponding to an area of 10 mm^2) as the characteristic element size. The energy release rate computed from the post-damage area under the uniaxial stress–strain curve and the selected element size is $\mathscr{G}_f = 17.5\ \text{MJ/m}^3 \times 3.175\ \text{mm} = 55.6\ \text{kJ/m}^2$. In other words, when fully damaged an element is capable of dissipating 55.6 kJ/m^2.

The experimental study by Delfosse and Poursartip (1997) has shown that for T800H/3900-2 CFRP when the fibre breakage is the only form of failure, the energy release rate (as estimated from three-point bend tests of unidirectional specimens) is $G_{\text{FD}} = 160 \pm 10\ \text{kJ/m}^2$. The energy release rate for matrix damage was also reported to be $G_{\text{MD}} = 5.0 \pm 0.5\ \text{kJ/m}^2$. According to our previously estimated quantities of fibre and matrix damage and the associated experimentally determined values of energy release rates, the energy release rate corresponding to a fully damaged sublaminate can be written as $0.75G_{\text{MD}} + 0.25G_{\text{FD}} \approx 44.0 \pm 2$ kJ/m^2. The latter is in reasonable agreement with the $\mathscr{G}_f$ value calculated above and demonstrates the consistency of the methodology presented here.

In summary, our approach has been shown to be physically justifiable and consistent with principles of damage mechanics, strength of materials and fracture mechanics. Fine tuning of the model parameters was not the object of the exercise here, rather the intent was to show the consistency of the approach using reasonable estimates of unknown parameters supported by available experimental measurements and observations.

References

ASTM, 2002. Annual Book of ASTM Standards—Space Simulation; Aerospace and Aircraft; High Modulus Fibers and Composites. ASTM, West Conshohocken, PA, USA.

Bakis, C.E., Stinchcomb, W.W., 1986. Response of thick, notched laminates subjected to tension–compression cyclic loads. In: Proceedings of Composite Materials: Fatigue and Fracture. Dallas, TX, USA.

Bazant, Z.P., Cedolin, L., 1991. Stability of Structures: Elastic, Inelastic, Fracture and Damage Theories. Oxford University Press, New York.

Bazant, Z.P., Oh, B.H., 1983. Crack band theory for fracture of concrete. Materials and Structures (RILEM, Paris) 16, 155–177.

Belytschko, T.B., Lin, J.I., Tsay, C.S., 1984. Explicit algorithms for the nonlinear dynamics of shells. Computer Methods in Applied Mechanics and Engineering 42, 225–251.

Belytschko, T.B., Bazant, Z.P., Hyun, Y.W., Chang, T.-P., 1986. Strain-softening materials and finite element solutions. Computers and Structures 23 (2), 163180.

Boeing, 1988. Advanced Composite Compression Tests: Boeing Specification Support Standard. The Boeing Company, Seattle, WA, USA.

Camponeschi, E.T., Stinchcomb, W.W., 1982. Stiffness reduction as an indicator of damage in graphite/epoxy laminates. In: Daniel, I.M. (Ed.), Composite Materials: Testing and Design, ASTM STP 787. ASTM, Philadelphia, PA, USA, pp. 225–246.

Chaboche, J.L., 1988a. Continuum damage mechanics. I. General concepts. Journal of Applied Mechanics 55 (1), 59–64.

Chaboche, J.L., 1988b. Continuum damage mechanics. II. Damage growth, crack initiation, and crack growth. Journal of Applied Mechanics 55 (1), 65–72.

Chang, F.K., Chang, K.Y., 1987. A progressive damage model for laminated composites containing stress concentrations. Journal of Composite Materials 21 (9), 834–855.

Chow, C.L., Wang, J., 1987. An anisotropic theory of elasticity for continuum damage mechanics. International Journal of Fracture 33, 3–16.

Delfosse, D., Poursartip, A., 1995. Experimental parameter study of static and dynamic out-of-plane loading of CFRP laminates. In: Proceedings of the Tenth International Conference on Composite Materials (ICCM/10). Whistler, BC, Canada, V583–V590.

Delfosse, D., Poursartip, A., 1997. Energy-based approach to impact damage in CFRP laminates. Composites 28A, 647–655.

Delfosse, D., 1994. Experimental results from static and dynamic out-of-plane loading of laminated composite materials. Joint Report to the Defence Research Establishment Valcartier (DREV) and the Directorate Research and Development Land (DRDL) of the Department of National Defence, Department of Metals and Materials Engineering, The University of British Columbia, Vancouver.

Delfosse, D., Poursartip, A., Coxon, B.R., et al., 1995. Non-penetrating impact behaviour of cfrp at low and intermediate velocities. In: Martin, R.H. (Ed.), Composite Materials: Fatigue and Fracture, ASTM STP 1230. ASTM, Philadelphia, PA, USA, pp. 333–350.

Dost, E.F., Ilcewicz, L.B., Avery, W.B., et al., 1991. Effects of stacking sequence on impact damage resistance and residual strength for quasi-isotropic laminates. In: O'Brien, T.K. (Ed.), Composite Materials: Fatigue and Fracture, ASTM STP 1110. ASTM, Philadelphia, PA, USA, pp. 476–500.

Floyd, A., Williams, K., Vaziri, R., Kanji, K., Poursartip, A., 1999. Through-thickness strain-softening damage modelling of composite laminates. In: Proceedings of the 18th International Symposium and Exhibition on Ballistics. San Antonio, Texas, pp. 877–884.

Floyd, A.M., Mitchell, J., Vaziri, R., Poursartip, A., 2001. Modelling damage development in overheight compact tension (OCT) specimens. In: Proceedings of the Thirteenth International Conference on Composite Materials (ICCM/13). Beijing, China.

Hallquist, J.O., Stillman, D.W., Lin, T-L., 1994. LS-DYNA3D User's Manual. Livermore Software Technology Corporation (LSTC), Livermore, CA, USA.

Hashin, Z., 1980. Failure criteria for unidirectional fiber composites. Journal of Applied Mechanics 47, 329–334.

Highsmith, A.L., Reifsnider, K.L., 1982. Stiffness-reduction mechanisms in composite laminates. In: Reifsnider, K.L. (Ed.), Damage in Composite Materials: Basic Mechanisms, Accumulation, Tolerance, and Characterization, ASTM STP 775. ASTM, Philadelphia, PA, USA, pp. 103–117.

Hinton, M.J., Soden, P.D., 1998. Predicting Failure in Composite Laminates: The Background to the Exercise. Composites Science and Technology 58 (7), 1001–1010.

Hinton, M.J., Kaddour, A.S., Soden, P.D., 2001. Predicting Failure in Fibre Composites: Lessons Learned from the World-Wide Failure Exercise. In: Proceedings of the Thirteenth International Conference on Composite Materials (ICCM/13). Beijing, China.

Hsu, P.W., Herakovich, C.T., 1977. Edge effects in angle ply composite laminates. Journal of Composite Materials 11, 422–434.

Hull, D., Legg, M.J., Spencer, B., 1978. Failure of glass/polyester filament wound pipes. Composites 9, 17–24.

Ilcewicz, L.B., 1992. Private Communication. The Boeing Company, Seattle, WA, USA.

Kachanov, L.M., 1958. On the Creep Rupture Time, Izv. AN SSSR, Otd. Tekhn, Nauk 8, 2631.

Kachanov, L.M., 1986. Introduction to Continuum Damage Mechanics. Nijhoff. Dordrecht, The Netherlands.

Kennedy, T.C., Nahan, M.F., 1997. A simple nonlocal damage model for predicting failure in a composite shell containing a crack. Composite Structures 39 (1–2), 85–91.

Kongshavn, I., Poursartip, A., 1999. Experimental investigation of a strain softening approach to predicting failure in notched fibre reinforced composite laminates. Composites Science and Technology 59 (1), 29–40.

Krajcinovic, D., 1984. Continuum damage mechanics. Applied Mechanics Review 37 (1), 1–6.

Krajcinovic, D., 1996. Damage Mechanics. In: Achenbach, J.D., et al. (Ed.), North-Holland Series in Applied Mathematics and Mechanics, Elsevier Science, vol. 41.

Kress, G.R., Stinchcomb, W.W., 1985. Fatigue response of notched graphite/epoxy laminates. In: Vinson, J.R., Taya, M. (Eds.), Recent Advances in Composites in the United States and Japan, ASTM STP 864. ASTM, Philadelphia, PA, USA, pp. 173–196.

Lafarie-Frenot, M.-C., Riviere, J.-M., 1988. Méchanismes D'Endommagement Par Fatigue D'Un Composite Stratifié à Fibre Longues: Étude De La Fissuration Transverse, In: Comptes-Rendus des Sixièmes Journé es Nationales sur les Composites. Paris, France, pp. 635–647.

Lagace, P.A., 1984. Notch sensitivity and stacking sequence of laminated composites. In: Composite Materials: Testing and Design, Seventh Conference. Philadelphia, PA, USA, pp. 161–176.

Laws, N., Brockenbrough, J.R., 1987. The effect of micro-crack systems on the loss of stiffness of brittle solids. International Journal of Solids and Structures 23 (9), 1247–1268.

Lemaître, J., Chaboche, J.L., 1978. Aspect Phé nomènologique De La Rupture Par Endommagement. Journal de Mé canique Appliquée 2 (2), 317–365.

Matzenmiller, A., Lubliner, J., Taylor, R.L., 1995. A constitutive model for anisotropic damage in fiber-composites. Mechanics of Materials 20 (2), 125–152.

O'Brien, T.K., Reifsnider, K.L., 1981. Fatigue damage evaluation in boron-epoxy laminates. Journal of Composite Materials 15, 55–70.

O'Brien, T.K., 1982. Characterization of delamination onset and growth in a composite laminate. In: Reifsnider, K.L. (Ed.), Damage in Composite Materials: Basic Mechanisms, Accumulation, Tolerance, and Characterization, ASTM STP 775. ASTM, Philadelphia, USA, pp. 141–167.

Ogin, S.L., Smith, P.A., Beaumont, P.R., 1985. Matrix cracking and stiffness reduction during the fatigue of a $(0/90)_s$ GFRP laminate. Composites Science and Technology 22 (1), 23–31.

Ortiz, M., 1985. A constitutive theory for the inelastic behavior of concrete. Mechanics of Materials 4, 67–93.

Pagano, N.J., Pipes, R.B., 1971. The influence of stacking sequence on laminate strength. Journal of Composite Materials 5, 50–57.

Pickett, A.K., Haug, E., Ruckert, J., 1990. A fracture damaging law suitable for anisotropic short fibre/matrix materials in an explicit finite element code. Composites 21 (4), 297–304.

Poursartip, A., Ashby, M.F., Beaumont, P.R., 1986. The fatigue damage mechanics of a carbon fibre composite laminate I—Development of the model. Composites Science and Technology 25 (3), 193–218.

SACMA, 1988. Recommended Test Method SRM 2-88. Suppliers of Advanced Composite Materials Association. Arlington, VA, USA.

Simo, J.C., Ju, J.W., 1987. Strain and stress-based continuum damage models—I. Formulation. International Journal of Solids and Structures 23 (7), 821–840.

Soden, P.D., Hinton, M.J., Kaddour, A.S., 1998. A comparison of the predictive capabilities of current failure theories for composite laminates. Composites Science and Technology 58 (7), 1225–1254.

Steif, P., 1984. Stiffness reduction due to fiber breakage. Journal of Composite Materials 17, 153–172.

Straznicky, P.V., Worswick, M.J., Majeed, O., et al., 1993. Impact damage in composite laminates. In: Proceedings of the Third International Conference on Composite Materials (ICCM/9), Madrid, Spain, pp. 386–393.

Talreja, R., 1985a. Transverse cracking and stiffness reduction in composite laminates. Journal of Composite Materials 19 (4), 355–375.

Talreja, R., 1985b. A continuum mechanics characterization of damage in composite materials. Proceedings of the Royal Society of London A 399 (1817), 195–216.

Tsai, S.W., Wu, E.M.A., 1971. General theory of strength for anisotropic materials. Journal of Composite Materials 5, 58–80.

Tsai, S.W., 1988. Composite design, think composites. Dayton, OH, USA.

Williams, K., 1998. A Physically-Based Continuum Damage Mechanics Model for Numerical Prediction of Damage Growth in Laminated Composite Plates. Ph.D. Thesis. Department of Metals and Materials Engineering, The University of British Columbia, Vancouver, BC, Canada.

Williams, K., Vaziri, R., 1995. Finite Element Analysis of the Impact Response of CFRP Composite Plates. In: Proceedings of the Tenth International Conference on Composite Materials (ICCM/10). Whistler, BC, Canada, V647-V654.

Williams, K., Vaziri, R., 2001. Application of a damage mechanics model for predicting the impact response of composite materials. Computers and Structures 79, 997–1011.

Williams, K., Floyd, A., Vaziri, R., Poursartip, A., 1999. Numerical simulation of in-plane damage progression in laminated composite plates. In: Proceedings of the 12th International Conference on Composite Materials (ICCM/12), paper 614, Paris, France.

Yazdchi, M., Valliappan, S., Zhang, W., 1996. A continuum model for dynamic damage evolution of anisotropic brittle materials. International Journal for Numerical Methods in Engineering 39, 1555–1583.